CRCLEME
Cooperative Research Centre for
Landscape Evolution & Mineral Exploration

OPEN FILE
REPORT
SERIES

CSIRO
EXPLORATION
AND MINING

AMIRA
Australian Mineral Industries Research Association Limited ACN 004 448 266

PETROGRAPHY, MINERALOGY AND GEOCHEMISTRY OF SOIL AND LAG OVERLYING THE LIGHTS OF ISRAEL GOLD MINE, DAVYHURST, WESTERN AUSTRALIA

Volume 1

I.D.M. Robertson and M.F.J. Tenhaeff

CRC LEME OPEN FILE REPORT 31

September 1998

(CSIRO Division of Exploration Geoscience Report 232R, 1992.
Second impression 1998)

AMIRA
Australian Mineral Industries Research Association Limited ACN 004 448 266

CRCLEME
Cooperative Research Centre for
Landscape Evolution & Mineral Exploration

CSIRO
EXPLORATION
AND MINING

PETROGRAPHY, MINERALOGY AND GEOCHEMISTRY OF SOIL AND LAG OVERLYING THE LIGHTS OF ISRAEL GOLD MINE, DAVYHURST, WESTERN AUSTRALIA

Volume 1

I.D.M. Robertson and M.F.J. Tenhaeff

CRC LEME OPEN FILE REPORT 31

September 1998

(CSIRO Division of Exploration Geoscience Report 232R, 1992.
Second impression 1998)

CRC LEME is an unincorporated joint venture between The Australian National University,
University of Canberra, Australian Geological Survey Organisation and CSIRO Exploration and Mining
Headquarters: CRC LEME c/o CSIRO Exploration and Mining, Private Bag, PO Wembley, Western Australia, 6014

RESEARCH ARISING FROM CSIRO/AMIRA REGOLITH GEOCHEMISTRY PROJECTS 1987-1993

In 1987, CSIRO commenced a series of multi-client research projects in regolith geology and geochemistry which were sponsored by companies in the Australian mining industry, through the Australian Mineral Industries Research Association Limited (AMIRA). The initial research program, "Exploration for concealed gold deposits, Yilgarn Block, Western Australia" (1987-1993) had the aim of developing improved geological, geochemical and geophysical methods for mineral exploration that would facilitate the location of blind, buried or deeply weathered gold deposits. The program included the following projects:

P240: Laterite geochemistry for detecting concealed mineral deposits (1987-1991). Leader: Dr R.E. Smith.
Its scope was development of methods for sampling and interpretation of multi-element laterite geochemistry data and application of multi-element techniques to gold and polymetallic mineral exploration in weathered terrain. The project emphasised viewing laterite geochemical dispersion patterns in their regolith-landform context at local and district scales. It was supported by 30 companies.

P241: Gold and associated elements in the regolith - dispersion processes and implications for exploration (1987-1991). Leader: Dr C.R.M. Butt.
The project investigated the distribution of ore and indicator elements in the regolith. It included studies of the mineralogical and geochemical characteristics of weathered ore deposits and wall rocks, and the chemical controls on element dispersion and concentration during regolith evolution. This was to increase the effectiveness of geochemical exploration in weathered terrain through improved understanding of weathering processes. It was supported by 26 companies.

These projects represented "an opportunity for the mineral industry to participate in a multi-disciplinary program of geoscience research aimed at developing new geological, geochemical and geophysical methods for exploration in deeply weathered Archaean terrains". This initiative recognised the unique opportunities, created by exploration and open-cut mining, to conduct detailed studies of the weathered zone, with particular emphasis on the near-surface expression of gold mineralisation. The skills of existing and specially recruited research staff from the Floreat Park and North Ryde laboratories (of the then Divisions of Minerals and Geochemistry, and Mineral Physics and Mineralogy, subsequently Exploration Geoscience and later Exploration and Mining) were integrated to form a task force with expertise in geology, mineralogy, geochemistry and geophysics. Several staff participated in more than one project. Following completion of the original projects, two continuation projects were developed.

P240A: Geochemical exploration in complex lateritic environments of the Yilgarn Craton, Western Australia (1991-1993). Leaders: Drs R.E. Smith and R.R. Anand.
The approach of viewing geochemical dispersion within a well-controlled and well-understood regolith-landform and bedrock framework at detailed and district scales continued. In this extension, focus was particularly on areas of transported cover and on more complex lateritic environments typified by the Kalgoorlie regional study. This was supported by 17 companies.

P241A: Gold and associated elements in the regolith - dispersion processes and implications for exploration. Leader: Dr. C.R.M. Butt.
The significance of gold mobilisation under present-day conditions, particularly the important relationship with pedogenic carbonate, was investigated further. In addition, attention was focussed on the recognition of primary lithologies from their weathered equivalents. This project was supported by 14 companies.

Although the confidentiality periods of the research reports have expired, the last in December 1994, they have not been made public until now. Publishing the reports through the CRC LEME Report Series is seen as an appropriate means of doing this. By making available the results of the research and the authors' interpretations, it is hoped that the reports will provide source data for future research and be useful for teaching. CRC LEME acknowledges the Australian Mineral Industries Research Association and CSIRO Division of Exploration and Mining for authorisation to publish these reports. It is intended that publication of the reports will be a substantial additional factor in transferring technology to aid the Australian Mineral Industry.

This report (CRC LEME Open File Report 31) is a first revision of CSIRO, Division of Exploration Geoscience Restricted Report 232R, first issued in 1992, which formed part of the CSIRO/AMIRA Projects P240A and P241A .

Copies of this publication can be obtained from:
The Publication Officer, CRC LEME, CSIRO Exploration and Mining, PMB, Wembley, WA 6014, Australia. Information on other publications in this series may be obtained from the above or from http://leme.anu.edu.au/
Bibliographic reference:
This publication should be referred to as Robertson, I.D.M. and Tenhaeff, M.F.J., 1998. Petrography, mineralogy and geochemistry of soil and lag overlying the Lights of Israel Gold Mine, Davyhurst, Western Australia. Open File Report 31, Cooperative Research Centre for Landscape Evolution and Mineral Exploration, Perth, Australia.
Cataloguing-in-Publication:
Robertson, I.D.M.
Petrography, mineralogy and geochemistry of soil and lag overlying the Lights of Israel Gold Mine, Davyhurst, Western Australia
ISBN v1: 0 642 28219 6 v2: 0 642 28220 X set: 0 642 28221 8
1. Geochemistry 2. Mineralogy 3. Gold - Western Australia.
I. Tenhaeff, M.F.J. II. Title
CRC LEME Open File Report 31.
ISSN 1329-4768

FRONTISPIECE

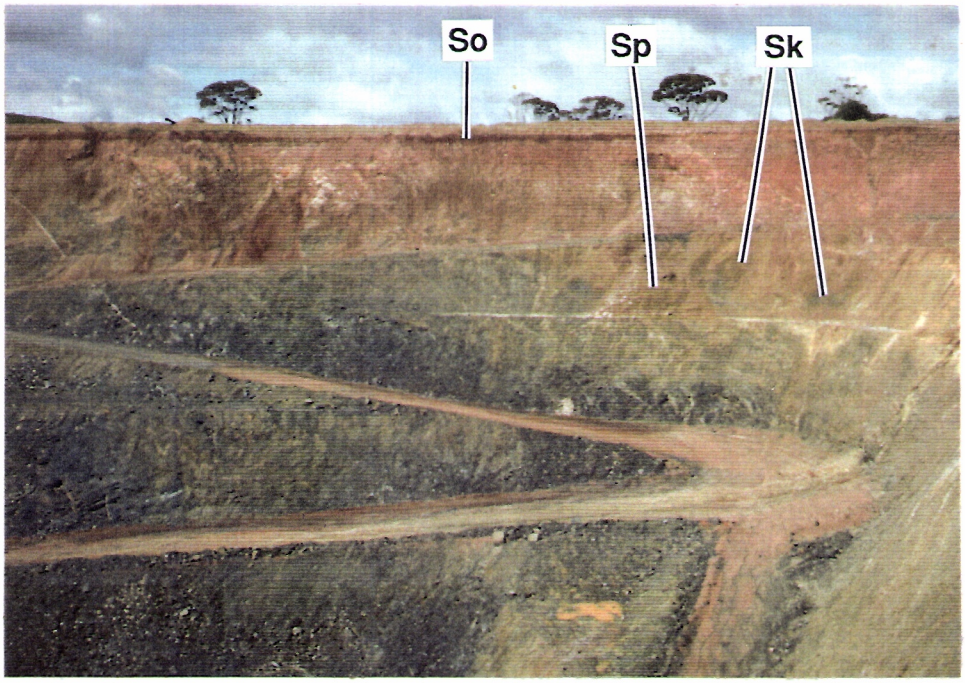

The south-east end of the lights of Israel Pit showing a considerably truncated weathered mantle. The depth to saprock is variable and fragments of saprock (Sk) are enclosed in brown saprolite (Sp). A thin soil (So) is developed over the saprolite.

PREFACE

The CSIRO - AMIRA Programme "Exploration for Concealed Gold Deposits, Yilgarn Block, Western Australia" has, as its overall aim, the development of improved geological, geochemical and geophysical methods for mineral exploration that will facilitate the location of blind, concealed or deeply weathered gold deposits.

Two of the projects within the programme (AMIRA P240A, Yilgarn Lateritic Environments and P241A, Weathering Processes) have collaborated for integrated studies at selected orientation sites. One of these is an integrated regolith study at the Lights of Israel Gold Mine, near Davyhurst, in the Coolgardie-Mt. Ida Greenstone Belt. This report describes the results of a mineralogical, petrographic and geochemical study of the soil and lag, carried out for both Projects P241A and P240A, using samples that were collected prior to mining. The site is south of the Menzies Line and has a surficial environment typical of the region, namely hypersaline groundwater, calcareous soils and eucalypt-dominated vegetation. It provides a valuable contrast with a similar study of the Beasley Creek Mine, at Laverton, in the north-eastern Goldfields, which is north of the Menzies Line, in an environment of fresh groundwater, mostly carbonate-poor soils and acacia-dominated vegetation. The outcome of the research demonstrates that regional effects must be taken into account in designing sampling strategies. At Beasley Creek, lag and ferruginous fractions of the soil are the most effective sample media for Au whereas, at Lights of Israel, the best response is given by the calcareous fractions. The study at Lights of Israel thus confirms the conclusion of other studies conducted by Projects P241 and P241A in this region. Petrographic study of the coarse lag reveals fabrics typical of mafic saprolites and some minor gossans, again demonstrating the potential of lag petrography for rock type identification.

C.R.M. Butt
Project Leader, P241A (Dispersion Processes)

R.E. Smith
Project Leader, P240A (Yilgarn Lateritic Environments)

October, 1992.

TABLE OF CONTENTS

LIST OF FIGURES

LIST OF TABLES

1.0 ABSTRACT

The Lights of Israel Mine Site lies in an erosional regime, where the weathered profile has been truncated to within the mottled zone. This study area, south of the Menzies Line, in an area of eucalypt woodland, where soil carbonates are common, provides a useful contrast with the arid environment of Beasley Creek to the north-east.

Samples of the lag and the generally thin, colluvial soil were collected along one traverse over the Lights of Israel Mine Site, prior to mining. The lag, the soil and its components have been examined petrographically, mineralogically and geochemically. The coarse fraction (>600 μm) consists of black, goethite- and hematite-rich nodules (some of which are magnetic), red to yellow, ferruginous clay granules, quartz fragments and scarce crystals of tourmaline and gossan fragments. All the ferruginous fragments are petrographically indistinguishable from the fine lag, which was formed by deflation of the top layers of soil. Some of the upper soil layers are rich in carbonates, contain crystals of pedogenic gypsum and curly crystals of halite.

The iron-rich fragments contain lithorelics, containing microscopic relics of layer silicates (smectites and kaolinite), set in, and largely replaced by, massive, spongy or vesicular goethite. The clay-rich granules consist largely of hematite- or goethite-stained kaolinite and some include goethite-rich lithorelics. Very close to the mineralisation, fragments of gossan, showing pseudomorphs after fine-grained pyrite, were identified in the lag. The soil contains a significant, quartz-rich, component which is largely angular and glassy and appears to be largely of local derivation. It is most abundant in the 75-710 μm fraction, where it acts as a geochemical diluent. There is a very minor aeolian component, which becomes progressively more abundant in the finer fractions. The silty fraction (<75 μm) contains less quartz but more iron oxides and clay. Its contained <4 μm fraction is very clay rich. The sandy and silty fractions contain a trace of sharp, fresh crystal fragments of tourmaline, which have a composition indistinguishable from that of local veinlet tourmaline.

The complete soil and the >600, the <75 and the <4 μm fractions were analysed to assess their value as sampling media. The quartz-rich 75-710 μm fraction was discarded. Gold in the fine soil fractions is the best guide to mineralisation by far. Very weak and equivocal anomalies in As, Sb, Cu and Cd are probably also ore related. Maxima in K and Rb seem to indicate a phyllic alteration halo around the mineralisation. The elevated S background above the mineralisation is problematical; its isotopic composition is slightly heavier than that which would be expected from meteoric S.

Gold anomalies are best developed in the calcareous soil fractions, are small and lack any extensive dispersion halo. Apart from Au the multi-element signature is weak and subtle and is likely to be overlooked by exploration. These conclusions contrast with those reached at Beasley Creek, north of the Menzies Line, where there is a strong multi-element signature and the best geochemical medium is the lag and the coarse, ferruginous fraction of the soil.

2.0 INTRODUCTION

A study of the Lights of Israel Gold Deposit, owned by Bardoc Gold Pty., Ltd., is being carried out within the CSIRO/AMIRA Yilgarn Gold Research Program. This deposit lies about 2 km north-east of Davyhurst at 120° 39' 45"E and 30° 01' 40"S (Figure 1A). Pre-production ore reserves of 415 000 tonnes at 4.2 g/t were outlined (Hellsten *et al.*, 1990).

2.1 Work Program

This mine site is south of the Menzies Line, in an area dominated by large eucalypts and soils rich in carbonates (Figures 2A, 3A and B). Lights of Israel has provided a contrast with the apparently sulphide-rich Beasley Creek Mine, which lies in the more arid Northeastern Goldfields, north of the Menzies Line, in an area dominated by acacias, hardpan and only patchily-developed calcretes. At Beasley Creek, a very similar, though more extensive, investigation has been completed (Robertson and Gall, 1988; Robertson and Churchward, 1989; Robertson, 1989; Robertson, 1990; Robertson, 1991). Comparisons will be drawn with Beasley Creek throughout the text.

The research comprised studies of the surface geology and geomorphology, the geochemistry of surface materials (soil and lag) and the geochemistry of, and dispersions in, the saprolite. This report covers the overall geomorphology and the geochemistry, petrography and mineralogy of the soil and lag. Geochemical investigations of two sections across the deposit from surface to 60 m depth is in progress and will be the subject of a future report. Surface materials (soil and lag) were collected along line 1200 mN in November 1987, when the mine was at an advanced assessment stage and mining was imminent.

2.2 The Potential of Surface Geochemistry at Lights of Israel

The orebody at Lights of Israel was discovered by drilling on the site of old workings. There has been no previous geochemical survey of surficial materials (soil and lag). In contrast to Beasley Creek, primary mineralisation is sulphide-poor, with little pathfinder element content. The multi-element geochemical response in the soil and in the lag have been assessed and compared to that of Beasley Creek. In particular, the strengths of the anomalies in the coarse soil fraction and their degree of dispersion needed to be compared to those of the compositionally similar fine lag. The quartz-rich, intermediate soil fraction was regarded as of little geochemical value. The <75 μm fraction is a commonly-used sampling medium, so it, also, was selected for a multi-element study. The included clay fraction contains a significant proportion of iron oxides (hematite and goethite), together with much kaolinite and some very fine-grained quartz. It could, in part, be wind-blown but geochemical evidence suggests that most is probably locally derived from disaggregated saprolitic material. Whatever the derivation of the clay fraction, its contained clays and iron oxides are all capable of adsorbing pathfinder elements, which may have been mobile in the landscape. In view of the findings at Beasley Creek, this very fine fraction seemed worthy of particular attention.

3.0 STUDY METHODS

This study necessitated the analysis of 56 lag samples for 30 elements and 56 soil samples for 38 elements, some elements being analysed in duplicate by different methods. Also numerous X-ray qualitative and semi-quantitative diffraction analyses were completed and 231 microprobe analyses. Details of the techniques used for this, the field sampling, fractionation of the soil samples, sample preparation and petrography follow.

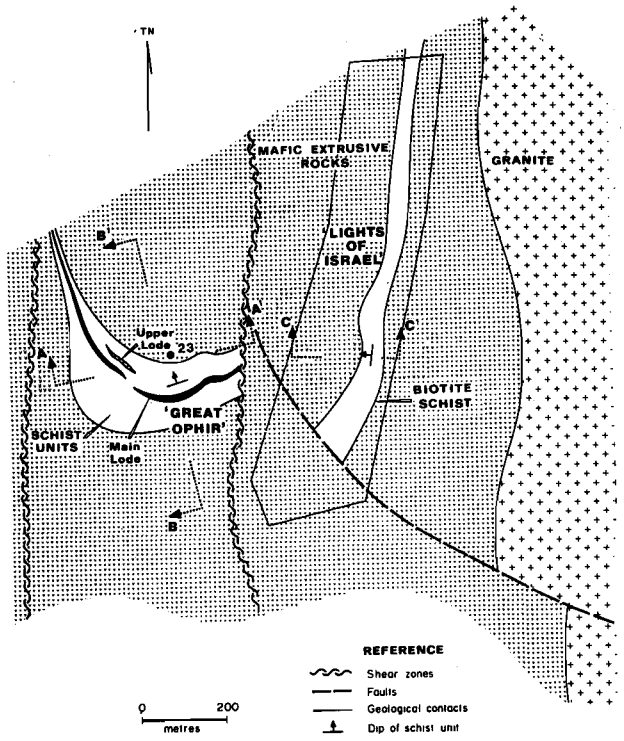

Figure 1A. Geological map of the environs of the Lights of Israel Gold Mine, Davyhurst (after Hellsten *et al.*, 1990)

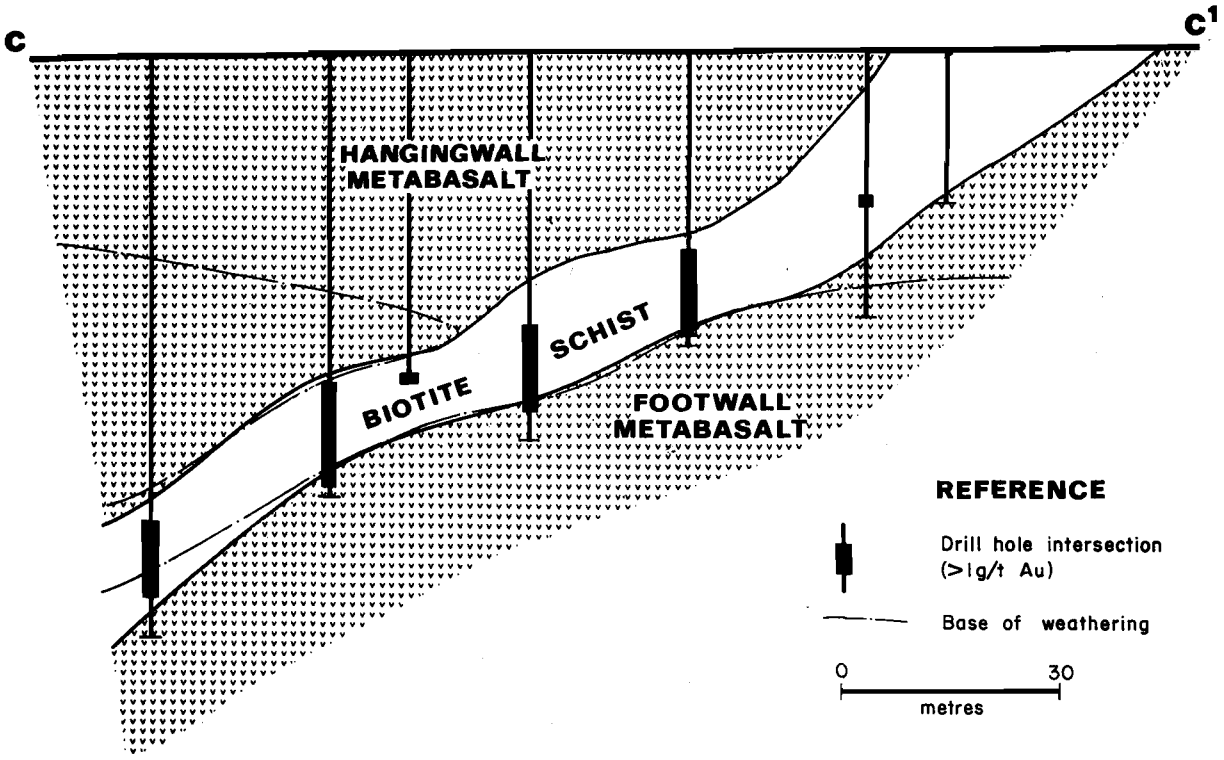

Figure 1B. Cross section, looking north, of the Lights of Israel Gold Deposit (after Hellsten *et al.*, 1990)

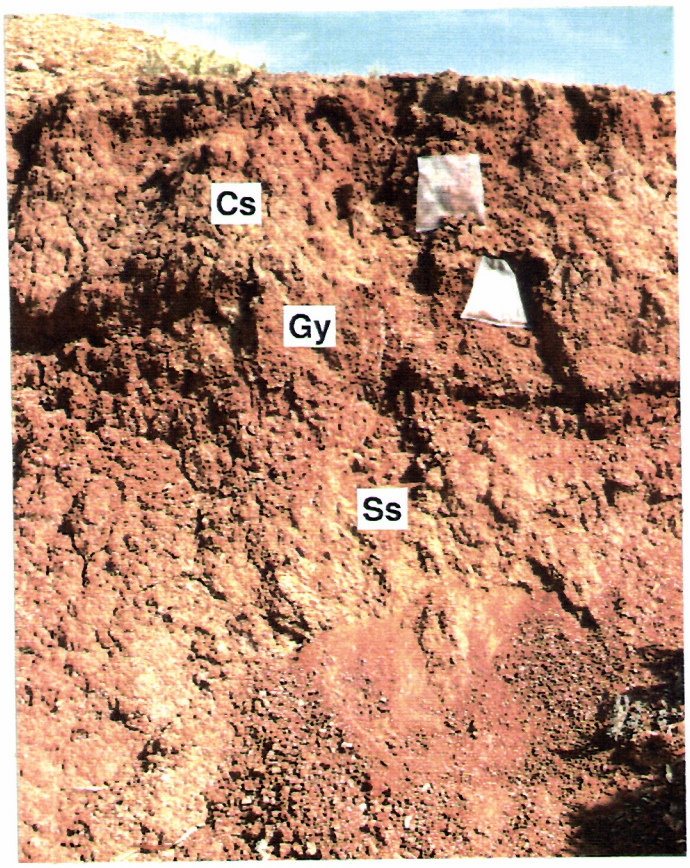

Figure 2A. A carbonate-rich soil (Cs) overlying a gypsiferous layer (Gy), which in turn is overlain by a carbonate-poor brown clay soil (Ss). Old stope on east side of pit (approx 1200 mE, 1210 mN).

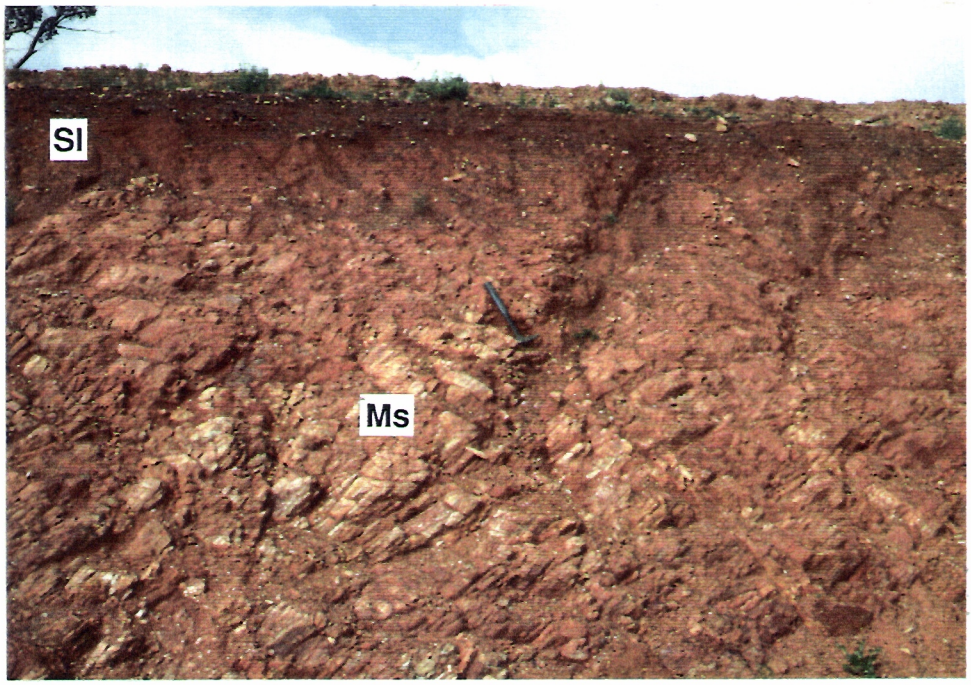

Figure 2B. A thin, lag-strewn residual soil (Sl) developed on cleaved mafic saprolite (Ms). South Access Ramp Lights of Israel Pit.

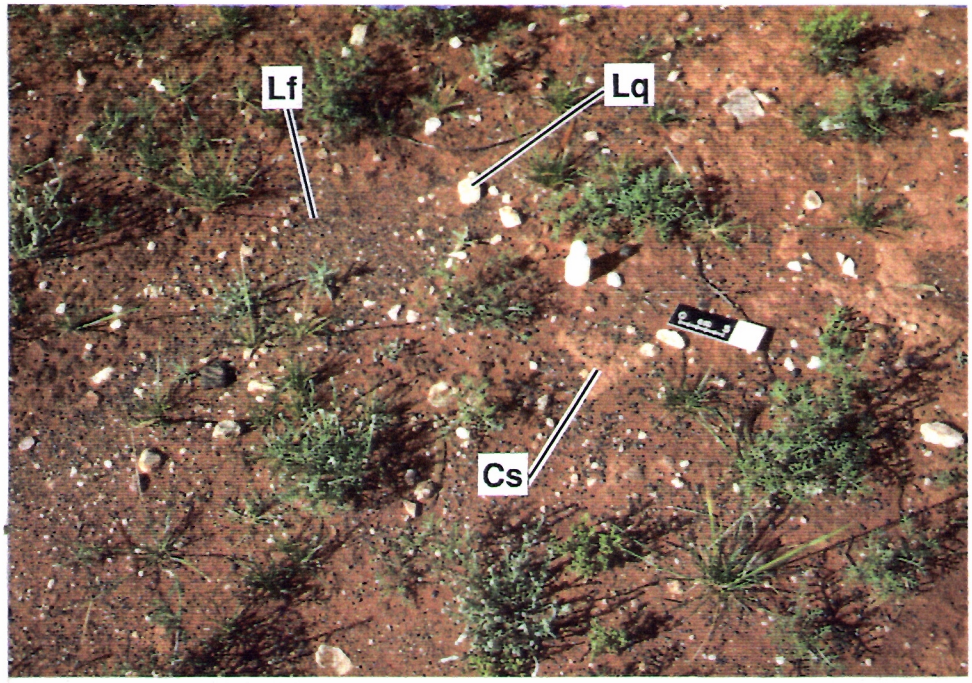

Figure 3A. A discontinuous, fine ferruginous lag (Lf), with common white quartz fragments (Lq) strewn over and partly masking a carbonate-rich soil (Cs). North of the pit.

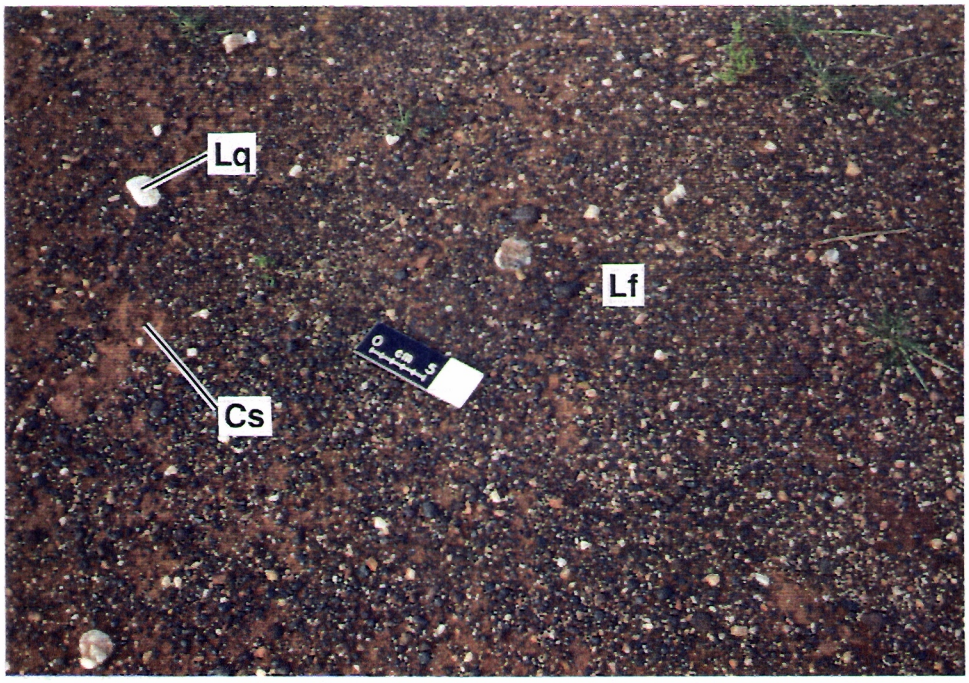

Figure 3B. A more abundant and coarser ferruginous lag (Lf) of mixed nodular material and ferruginous saprolite, with minor quartz (Lq), masking a carboante-rich soil (Cs). East of the south end of the pit.

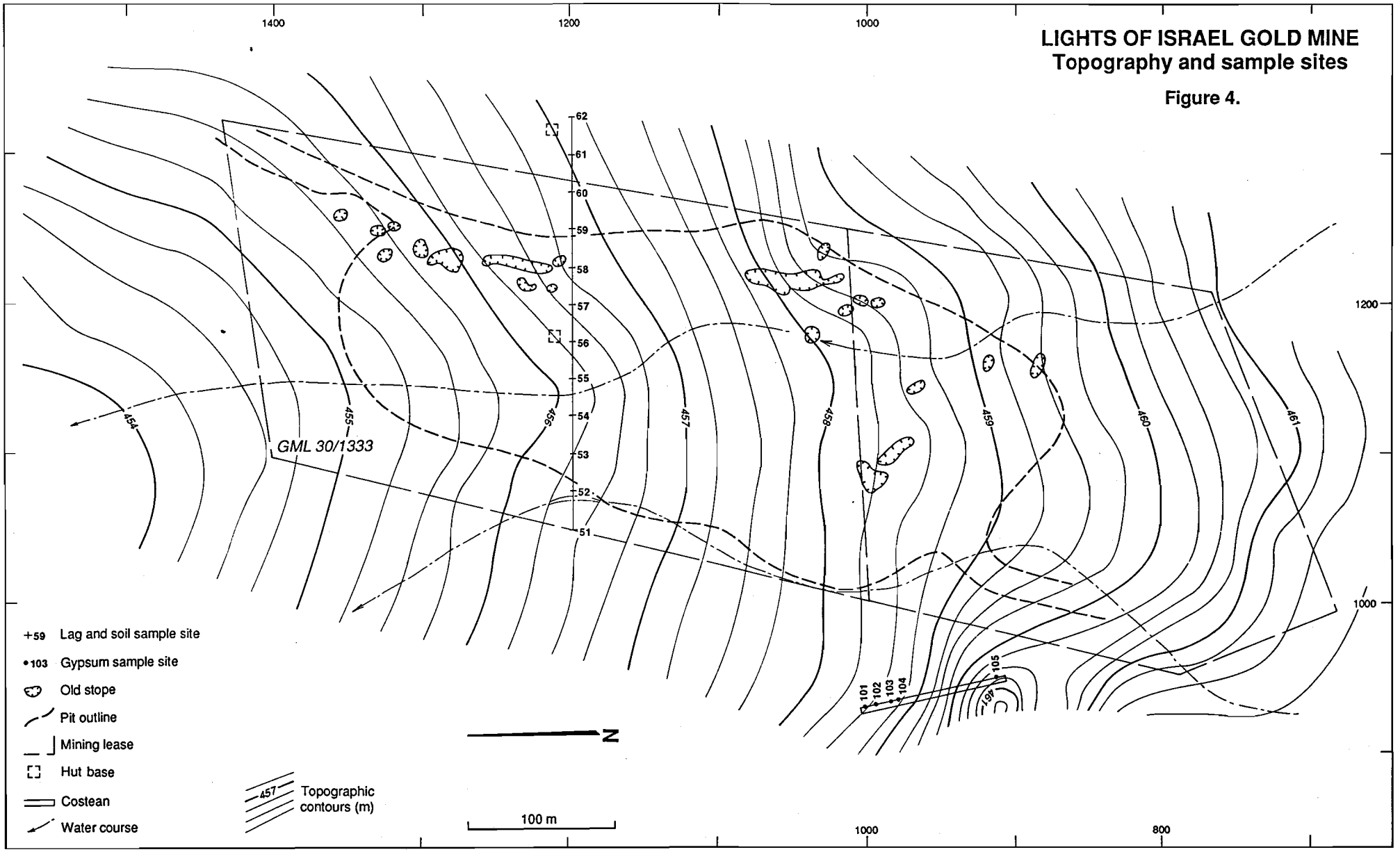
LIGHTS OF ISRAEL GOLD MINE
Topography and sample sites
Figure 4.
1400
1200
1000
800
1200
1000
62
61
60
59
58
57
56
55
54
53
52
51
454
455
456
457
458
459
460
461
GML 30/1333
101
102
103
104
105
N
100 m
+59 Lag and soil sample site
•103 Gypsum sample site
Old stope
Pit outline
Mining lease
Hut base
Costean
Water course
457 Topographic contours (m)

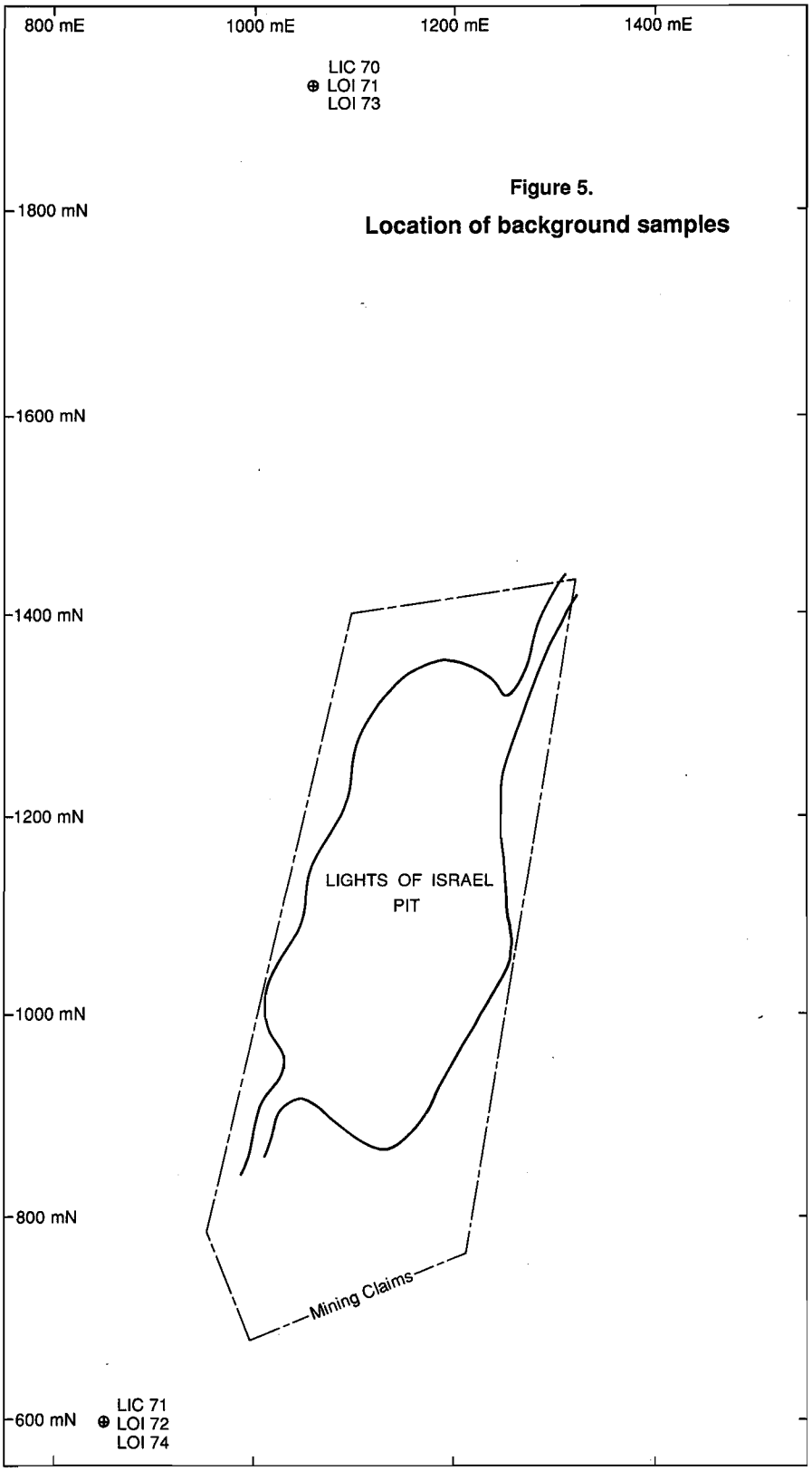

Figure 5.

Location of background samples

3.1 Natural Land Surface

An accurate plan of the topography was produced to aid data interpretation, based on 130 survey points within the mining lease. These were digitised from Plan No PLS/SM 13/4 (Bardoc Gold Pty., Ltd., 1987). To establish the topography as it was prior to human disturbance; survey points that were close to old stopes were ignored, where ground subsidence may have modified the surface. The data were gridded and contoured by computer and a contour plan produced at 0.25 m intervals (Figure 4).

3.2 Lag and Soil Sampling

Soil and lag samples were collected along line 1200 mN, which passed over the centre of the mineralisation. The soil samples were collected approximately coincident with lag samples at 25 m intervals. As extensive drilling had been carried out and there was some disturbance to the natural surface by vehicle tracks etc., care was taken in selecting undisturbed and uncontaminated sample sites. Where lag was scarce, or where the sample site was disturbed or contaminated, the area of search was extended up to 5 m along the sample line and up to 10 m across the line (along strike). The coarse lag samples (500-1000 g) were collected by hand. Only dark, dense, shiny lag fragments (10-50 mm) were sampled, discarding quartz and fragments of unferruginised saprolite. The fine lag samples (1000-1500 g) were swept into a plastic dustpan, with a nylon-bristled brush, from several randomly selected locations, within a similar area to that used for the coarse lag sampling. The fine lag sample inevitably contained some organic litter, soil and sand, which were later removed.

At each sample site, the upper 25 mm of soil were swept away to remove any contamination from the assessment drilling. A small hole, 150-250 mm deep, was excavated and about 1 kg of soil was collected and bagged in polythene. Background lag and soil sample sites were selected remote from the mineralisation, one to the north and one to the south. Their locations are shown in Figure 5. The pH of the soil was later recorded in the laboratory by pH meter, after shaking 2 g of the soil pulp with 10 ml of 0.01 M $CaCl_2$ and allowing the clays to settle for 2 or more hours.

3.3 Preparation of Lag

The *coarse lag* samples were washed with tap water on a 4 mm plastic sieve, to remove any dust or organic debris, and dried at $<50^{o}C$. Washing was essential, in view of the percussion drilling that had been carried out in the area. A small, representative sub-sample was selected by hand for reference, and later petrographic examination, and the remainder jaw crushed to a nominal <12 mm. A 100-150 g aliquot was riffle split from the jaw-crushed material and pulped to a nominal <75 µm in a case-hardened steel mill (Robertson and Crabb, 1988), using a double sand clean and alcohol wipe of the mill components between samples.

The *fine lag* samples were wet seived to >600 µm in tap water. Organic litter, sand and clay particles, adhering to the polished surfaces of the lag, were removed by agitation during sieving. The lag was dried at $<50^{o}C$. The result was a very clean product, which was riffle split into three parts. One part was retained for reference, one was pulped to <75 µm for analysis of the whole fine lag and the third part was separated, using a Sepor Automagnet, into magnetic and non-magnetic components, which were then pulped to <75 µm for analysis.

3.4 Preparation of Soil

After a size fraction pilot study (Appendix 18) on two representative samples, one from a point distant from the mineralisation (Sample LIC-53) and one from near the mineralisation (Sample

LIC-58) and examination of these fractions, a suitable preparation scheme was designed to yield samples of whole soil and three useful size fractions from the complete sample set.

A 2000-600 μm fraction was produced with adhering clays removed by ultrasonic cleaning. The 600-75 μm fraction was discarded after removal of all fines by wet sieving. The <75 μm fraction had its clay fraction (<4 μm) removed by sedimentation in water under pH control and both fractions were dried and analysed. Details of the soil fractionation techniques, modified from those of Robertson (1990) are given in Appendix 18.

3.5 XRD Mineralogy

Qualitative Analysis. All the complete soil samples and all the <4 μm fraction samples were examined by XRD at Floreat Park using a Philips PW1050 diffractometer, fitted with a graphite crystal diffracted beam monochromator. CuKα radiation was used for both qualitative and semiquantitative analysis. Each sample was scanned over the range 5-65° 2θ at a speed of 1° 2θ/min and data were collected at 0.02° 2θ intervals. Mineralogical compositions were determined by comparison with JCPDS files and laboratory standards.

Semi-quantitative analysis. Mineral abundances were estimated using the height above background of a selected XRD peak for each mineral (Table 1). The measured peaks were chosen so as to avoid overlap by peaks of other minerals. It must be emphasised that these results are approximate and are influenced by the degree of crystallinity, mass absorption of the sample, mineral orientation and abundance. Because of the wide variation in Fe contents, particularly between the ferruginous >600 μm fraction and the siliceous fine fractions, the results were corrected for mass absorption by the method of Brindley (1980). The data are in arbitrary units, which give a rough comparison of the relative abundances of *particular* minerals *between* samples; they do not indicate the relative abundances of the different minerals in each sample.

TABLE 1
Diffraction Peaks Used For Semi-Quantitative Mineralogy

Mineral	Diffraction peak (hkl)	d-Spacing (Å)
Quartz	101	3.34
Hematite	110	2.51
Goethite	110	4.18
Maghemite	220	2.95
Kaolinite	001	7.10
Calcite	002	3.03

3.6 Geochemical Analysis

The geochemical analysis of the lag was performed in November 1988, when major elements were currently determined by ICP analysis. The soil was not separated into its fractions until mid 1991; this was delayed, pending development of techniques for Beasley Creek. In 1991, improved major element analysis was available, by fused disc XRF, and also very sensitive ICP/MS techniques could be performed for Bi, Cd, In and Sn. Thus, in minor part, different techniques were used for these contrasting data sets. Methods used for the analysis of each trace element are given below. Detection limits are given in Appendix 1.

Samples were analysed as follows:

A. Neutron activation analysis (INAA), 30 g aliquots except for some clays where 10 g used (Becquerel Laboratories Pty. Ltd.): As, Au, Ce, Co, Cr, La, Mo, Sb, W.

B. X-Ray fluorescence (XRF(p)) on pressed powders, using a Philips PW1220C by the methods of Norrish and Chappell (1977) and Hart (1989), with Fe determined for matrix correction (CSIRO): Ba, Ce, Cu, Ga, Ge, Mn, Nb, Ni, Pb, Rb, Sr, V, Y, Zn, Zr.

C. X-Ray fluorescence (XRF(f)) of fused discs (0.7 g sample and 6.4 g Li borate) using a Philips PW1480 instrument by the method of Norrish and Hutton (1969) (CSIRO): Si, Al, Fe, Mg, Ca, Na, K, Ti, P, Ba, Ce, Co, Cr, Cu, Ga, La, Nb, Ni, Pb, Rb, Sr, V, Y, Zn, Zr. Soil only.

D. Inductively coupled plasma emission spectrometry (ICP-ES) on a Hilger E-1000 following fusion of 0.25 g samples with Li metaborate and solution in dilute HNO_3 (CSIRO): Si, Al, Fe, Mg, Ca, Ti, Ba, Be, Cr, Cu, Mn, Ni, V, Zr. Lag only.

E. Inductively-coupled plasma mass spectrometry (ICP-MS), following digestion with hot HCl, HF and $HClO_4$ and solution in HCl (Analabs): Ag, Cd, In, Sn, Bi. Soil only.

Readily-soluble Au was determined on the complete soils by iodide extraction (Gray *et al.*, 1990). An extracting reagent of 0.1 M potassium iodide and 1M sodium hydrogen carbonate, saturated by bubbling with CO_2, was first prepared and taken to pH 7.4 with hydrochloric acid. This reagent was shaken with 10 g of sample (< 75 μm pulp) for one day, at a soil/solution ratio of 1:2. The suspension was centrifuged (3000 rpm for 15 minutes) and the solution decanted (CSIRO) and analysed for Au by ICP-MS (Sheen Analytical Pty. Ltd).

The geochemical data for the complete soil and each of three soil fractions, comprising 10 major and 28 trace elements, are tabulated in Appendix 1, displayed graphically in Appendix 3 and are shown as frequency distribution plots in Appendices 4-7. The geochemical data for the coarse lag, the fine lag and its magnetic and non-magnetic components, comprising six major and 24 trace elements, are tabulated in Appendix 2, displayed graphically in Appendix 3 and are shown as frequency distribution plots in Appendices 8-11.

3.7 Sequencing and Standards

The samples were analysed in random order and in-house weathered rock standards (STD 8 and STD 9 for soils and STD 9 for lag) were introduced into the analytical batches at a ratio of 1:10 to 1:15, to monitor both accuracy and precision. The performance of the analytical method in relation to these standards, together with their mean values, standard deviations and the currently accepted values for these standards are reported in Appendices 1 and 2. The results are satisfactory in terms of both accuracy and precision.

3.8 Petrography

Ultrasonically cleaned samples of all size fractions of the soils, except the clays and < 75 μm fraction, were obtained and each examined under the binocular microscope. Thin and polished sections were prepared of most of the soil fractions and polished sections were prepared from pieces of the coarse lag. The polished sections were examined using both normally reflected and oblique illumination.

3.9 Microprobe Analysis

The compositions of tourmaline in the soils were compared with those in fresh rock to determine their possible source. Two samples of about 50 grains each were picked with tweezers from the 500-710 μm fraction of soil samples LIC-53 and LIC-58. Any extraneous magnetic material was removed and the tourmaline grains were mounted in resin and polished. These data were compared with tourmalines from a fresh quartz-tourmaline veinlet, collected from the pit (sample LOI-113).

The Cameca SX-50 microprobe at Floreat Park was used to analyse the tourmalines in wavelength dispersive mode, utilising a 30 nA beam, an accelerating voltage of 15 kV and a counting time of 20 s per element. Three garnets were used as secondary reference standards; the results of this standardisation is shown in Appendix 14 and indicate very reliable analyses. The major elements (Si, Al, Fe, Na, K, Ca and Ti) and some minor elements (Cr and Mn) were determined. A few analyses showed contamination with inclusions of quartz and sphene; these were eliminated. In all, 87 satisfactory tourmaline analyses were made from sample LIC-53, 66 analyses from sample LIC-58 and 53 from LOI-113. The core and rim of each grain was analysed and a short traverse was made across one grain to test for zoning, which was not found. Microprobe analysis was performed under the control of the WANU-SX geo-analytical package.

4.0 GEOLOGY, GEOMORPHOLOGY AND REGOLITH

4.1 Geology

The sub-surface geology, as determined by Bardoc Gold Pty., Ltd., largely from percussion drilling, is illustrated in Figures 1A and B. The mineralised zone is a strongly laminated plagioclase-biotite-amphibole schist, some 15-20 m thick (>0.5 g/t Au), which dips at 10-40° to the west and strikes north-northeast for over a kilometre. At its south end, it appears to be truncated by a north-west trending fault; the mineralised zone thins to the north, where its Au grade declines. Within it are two sub-parallel, high-grade zones (>2 g/t Au). Where fresh, it is a low-sulphide deposit with sulphide contents of 1-3% (pyrite and traces of chalcopyrite) and the abundances of pathfinder elements (As, W, base metals) are low. The mineralised zone does not outcrop at all, except in old stopes, and is variably weathered to 40-50 m depth.

The wall rocks are tholeiitic metabasalts, now metamorphosed to the amphibolite facies, with minor interflow sediments and dolerite, which have been intruded by felsic dykes and small quartz-tourmaline veinlets. Intrusive granitoids lie 200-400 m to the east. This suite of rocks comprises the Eastern Sequence of this part of the Coolgardie-Mount Ida segment of the Norseman-Wiluna Greenstone Belt and also contains the nearby Great Ophir and Golden Eagle gold deposits (Figure 1A).

4.2 Geomorphology and Regolith

The Lights of Israel Mine Site is located on a very gently undulating erosional plain. Here low, smooth, broadly convex crests rise some 2 m above shallow, broad swales and associated drainage floors. The area is mantled by open eucalypt woodland with shrubs of bluebush beneath. The eastern part of the mine site is on a slight rise and the axis is drained to the north by a small stream. The area of the mine site forms a very shallow valley which slopes gently (<1:100) to the north. The total relief is about 7 m. Two small streams are incised very slightly into this surface.

FIGURE 6
Lag And Soil Components

A. Laths and cross sections of subhedral, strongly birefringent tourmaline (schorl, Tm) in a groundmass of granular quartz (Qz), highly sausseritised plagioclase (Pl) and minor epidote. Crossed polarizers. Specimen LOI-113; 1060 mE 1020 mN 414 R.L.

B. Angular, ferruginous coarse lag fragments of highly ferruginised saprolite.

C. Components of the fine lag, separated by hand. Black, shiny, largely magnetic granules consisting of hematite and hematitic goethite (Hm), yellow-brown granules and nodules of goethite-stained kaolinitic clay (Kg), red-brown nodules of hematite-stained kaolinitic clay (Kh) and a variety of white, yellow and clear buck to druzy quartz (Qz).

D. The >600 μm component of the fine lag, which consists of dominant hematite-goethite granules (Hm), red-brown clay nodules (Kh) and angular quartz chips(Qz).

E. Fibrous, columnar and curly crystals of halite (Ha) from the carbonate-rich soil of sample LOI-001. One has attached soil (So). These halite whisker are probably formed by evaporation of salty soil pore fluids into soil voids.

F. The 142- 250 μm fraction consists largely of granules of quartz. Some are coated with hematite (Qh) and a very few are rounded by aeolian action (Qa). Most are uncoated, angular and glassy (Qz), suggesting a local origin.

G. Brown, well-formed crystals of pedogenic gypsum, below soil sample LOI-001.

H. Very angular fragments of clear quartz (Qz), largely uncoated, a few black, hematitic granules (Hm) and a chip of tourmaline (Tm) from the 250-500 μm soil fraction. This illustrates the local derivation of much of the soil quartz. Thin section, plane polarized transmitted light.

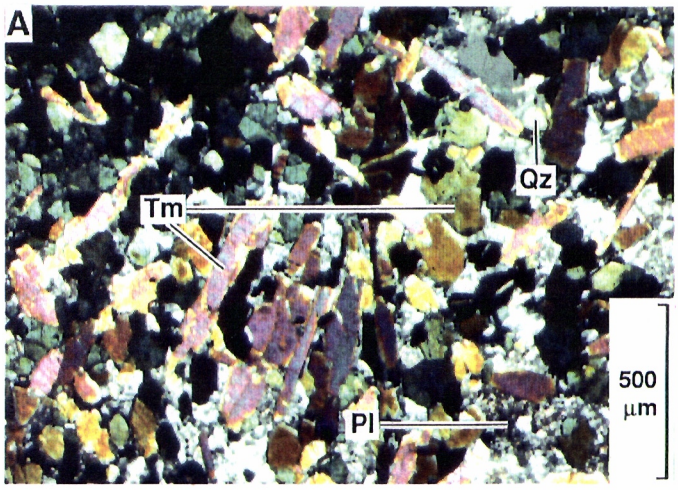
A
Qz
Tm
Pl
500
µm


B
5cm


C
Kg
Hm
Kh
Qz
2cm

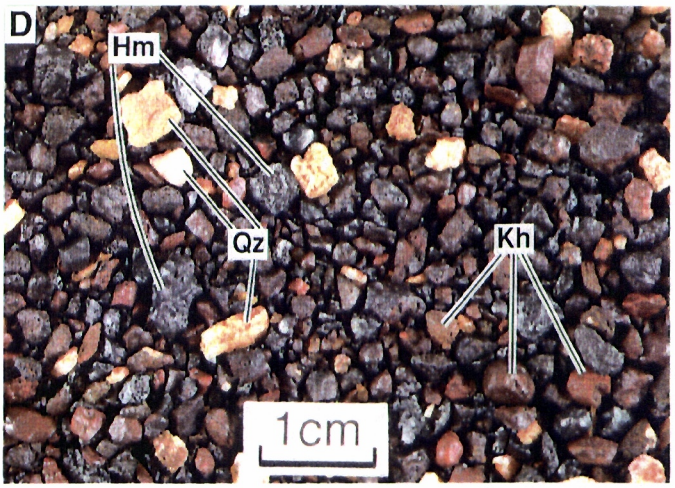
D
Hm
Qz
Kh
1cm

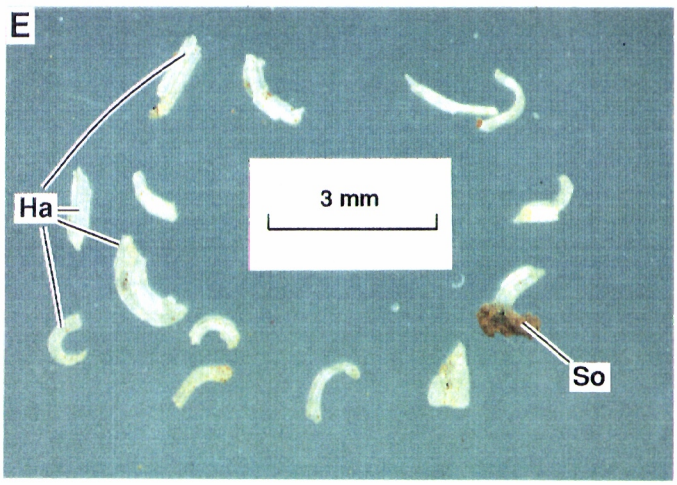
E
Ha
3 mm
So

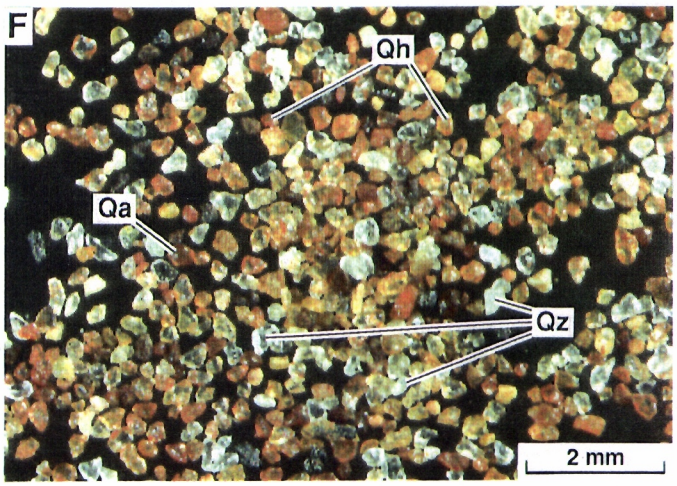
F
Qh
Qa
Qz
2 mm

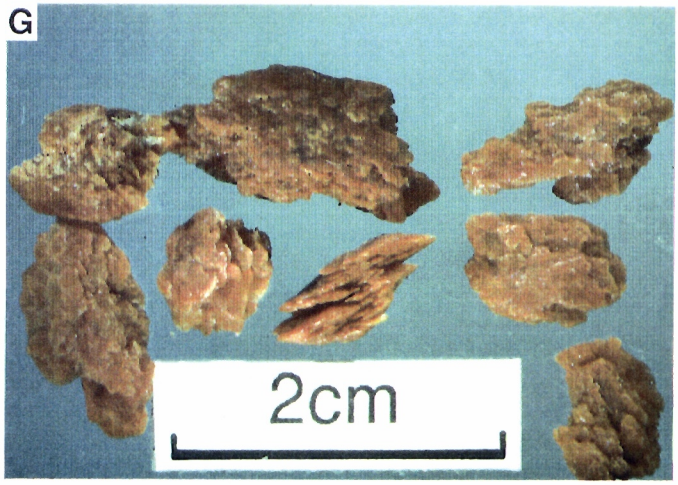
G
2cm

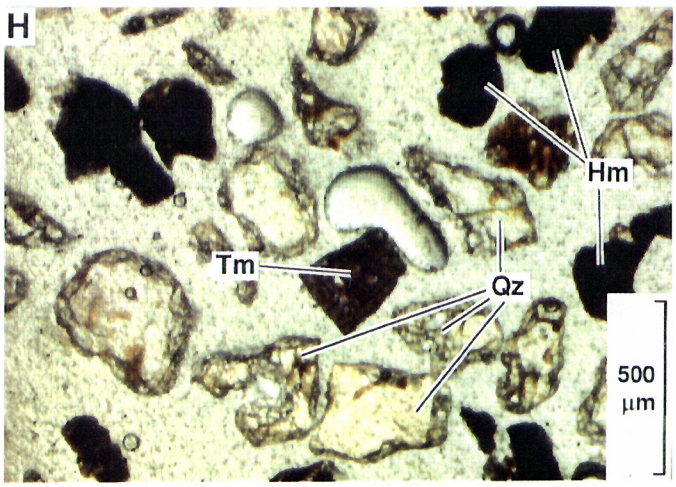
H
Hm
Tm
Qz
500
µm

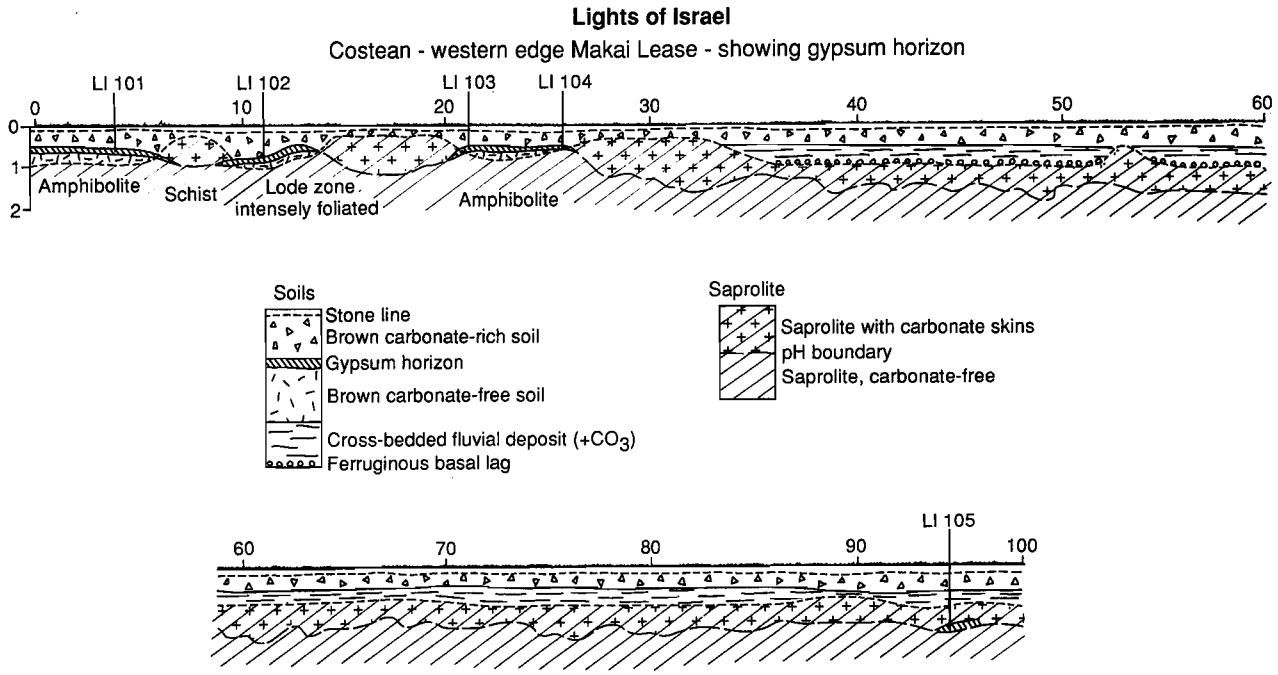
Lights of Israel
Costean - western edge Makai Lease - showing gypsum horizon
LI 101
LI 102
LI 103
LI 104
LI 105
0
10
20
30
40
50
60
70
80
90
100
0
1
2
Amphibolite
Schist
Lode zone
intensely foliated
Amphibolite
Soils
Stone line
Brown carbonate-rich soil
Gypsum horizon
Brown carbonate-free soil
Cross-bedded fluvial deposit (+CO3)
Ferruginous basal lag
Saprolite
Saprolite with carbonate skins
pH boundary
Saprolite, carbonate-free

Figure 7.

The weathering profile at the Lights of Israel Mine has been considerably truncated to below the mottled zone (Frontispiece) and a new, residual soil has developed from saprolite (Figure 2B). Parts of the soil profile have been eroded and minor fluvial material has been subsequently deposited. The wallrocks to the mineralisation are variably weathered to 20-30 m depth, the thickness of saprock varies considerably and blocks of saprock may be seen, in the side of the pit, enclosed in brownish saprolite (Frontispiece). Weathering penetrates much deeper where mineralisation occurs (Figure 1B).

The upper part of the regolith is a friable, red earth (clay loam to light clay) with soft carbonate from about 200 to 700 mm depth. Beneath this, the carbonate is largely confined to discrete pockets and even these are absent at 1.5 m. Under the swales, the soil is succeeded by a red, plastic clay that merges with saprolite at about 2 to 4 m. Beneath the low rises, this soil profile merges laterally to a light-brown, calcareous earth that also merges at depth with saprolite within 1 m of the surface.

Old stopes show the outline of the subcrop of the mineralisation (Figure 4). Two hut bases were recorded close to the sampled line (1200 mN) as possible sources of geochemical contamination and, in one fine lag sample, a 0.22" brass cartridge case was found.

Drilling in the area to the east of the pit (1000 mN, 1100 mE; 1150 mN, 1120 mE) indicated water at a depth of 48-52 m. Although no water analyses are available, the ground water would be expected to be hypersaline.

4.3 Soil

All the Archaean rocks at the Lights of Israel mine site were deeply weathered to saprolites and completely mantled by soil and lag (Frontispiece, Figures 2B, 3A and B). The west-dipping lode subcropped along the eastern side of the mine site and was marked by a line of small shafts and stopes (Figure 4) in which the ore zone, a biotite-kaolinite-quartz schist, was exposed between walls of weathered mafic schist. These stopes and shafts also exposed the soil profile (Figure 2A). At the top was a thin scattering of fine, iron-rich lag. This was underlain by about 600 mm of structureless, carbonate-rich, brown soil with small, ferruginous nodules. The carbonate-rich soil contained a few, small, white, fibrous, curled crystals (Figure 6E) of halite, with admixed clay, gypsum and iron oxides. Below this was a discontinuous gypsiferous horizon which consisted of coarse, decussate gypsum crystals (Figure 6G) with classic swallowtail twins, 5-20 mm in size, in a red-brown clay, overlying a carbonate-free soil and saprolite. A surface to 1 m ditchwitch trench, along line 1200 mN, showed that gypsum was abundant in the soil from 1165-1280 mE but it was apparently absent west of 1165 mE.

The gypsum in a costean exposure (150 m long) to the south-west of the planned pit (Figure 4), near the Great Ophir Mine, was examined in detail (Figure 7). The gypsum horizon (200 mm thick in places) occurs at the base of the carbonate-rich soil horizon (about 1 m thick), which is in turn underlain by carbonate-free soil (300 mm) and by saprolite. The development of carbonate is not limited to the soil. Where the saprolite nears the surface, carbonate forms skins on saprolite blocks; at the base of this, crystals of gypsum occur sporadically, just below the zone of carbonate. A shallow palaeochannel is exposed in the southern part of the costean (Figure 7), filled with cross-bedded fluvial gravels and sand, with a dark, ferruginous lag at the base. Although the palaeochannel sediments are carbonated, the regolith pH boundary, with its discontinuous gypsiferous horizon, passes below this palaeochannel. The formation of carbonate, and possibly gypsum as well, post-date the palaeochannel.

4.4 Lag

The soil is mantled discontinuously by matt, black, ferruginous, granular lag (Figures 3A and B) but it becomes progressively scarce to absent to the east of the mine site. These granules are scattered throughout the calcareous clay soils (Figure 3A) and the red, non-plastic clay soils beneath. The lag consists of a relatively scarse, coarse component (> 10 mm), making sample collection tedious, but the fine component is abundant. The coarse component is not a glossy, subrounded, nodular lag, like that from Beasley Creek, but angular, ferruginised fragments (Figure 6B) with a matt, slightly porous surface with inclusions of quartz and minor carbonate cement. They are probably best described as ferruginised rock fragments or ferruginised saprolite (LG231; Anand *et al.*, 1989). A minor lag component (5%) is fragments of white vein quartz, 10-40 mm in size (Figures 3A and B).

The fine lag (Figure 6D) consists dominantly (95%) of fragments of ferruginised saprolite with a few glossy black granules. Some ferruginised saprolite fragments are deep brown and some granules are yellow, possibly derived from a pre-existing duricrust (Figure 6C). Shard-like quartz fragments, which vary from white, buck quartz to clear or yellowish glassy and druzy quartz (Figure 6C) contribute 5% of the fine lag.

5.0 SOIL COMPOSITION

The results of a pilot size fraction analysis are briefly described and then the compositions of these fractions are investigated. This gives an insight into the origin of the soil components and helped in the design of the sample preparation method.

5.1 Soil Size Fractions

Two samples were selected for a pilot study from line 1200 mN; LIC-53 and LIC-58. One was selected as having been close to mineralisation (LIC-58) and the other relatively distant from it, so as to be as representative as possible of the whole suite. Seven size fractions were separated by sieving. The <4 μm fraction was partly extracted from the <75 μm fraction by sedimentation (Section 3). The percentage yields are presented in Table 2 and are shown graphically in Figure 8A.

TABLE 2
Soil Orientation Size Fraction Analysis

	LIC-53 Wt %	LIC-58 Wt %
>2000 μm	8.97	1.03
2000-710 μm	6.92	3.30
710-500 μm	3.16	2.51
500-250 μm	6.33	6.08
250-142 μm	11.32	18.42
142-75 μm	10.20	14.18
75-4 μm	32.50	34.28
<4 μm	20.59	20.19

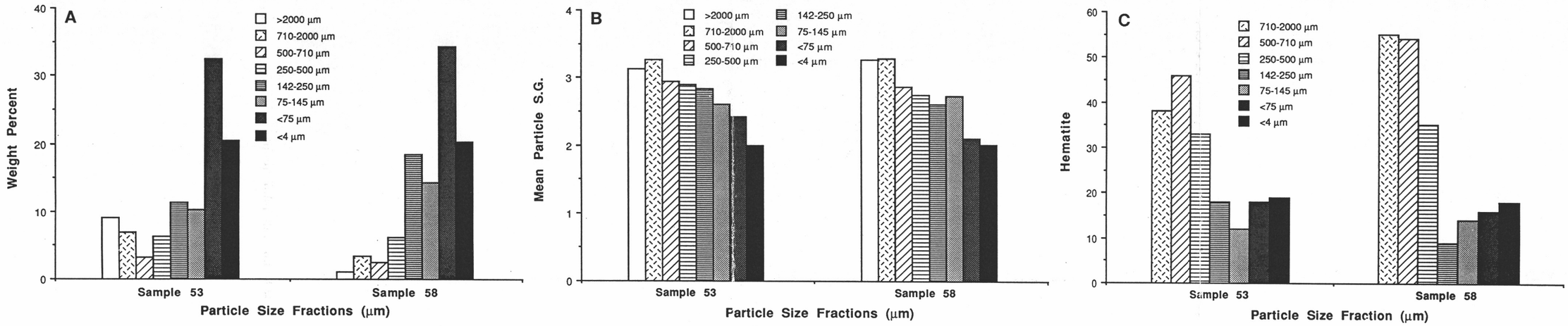

Figure 8. Distributions of abundance, particle density and mineralogical abundance of size fraction of pilot study samples.

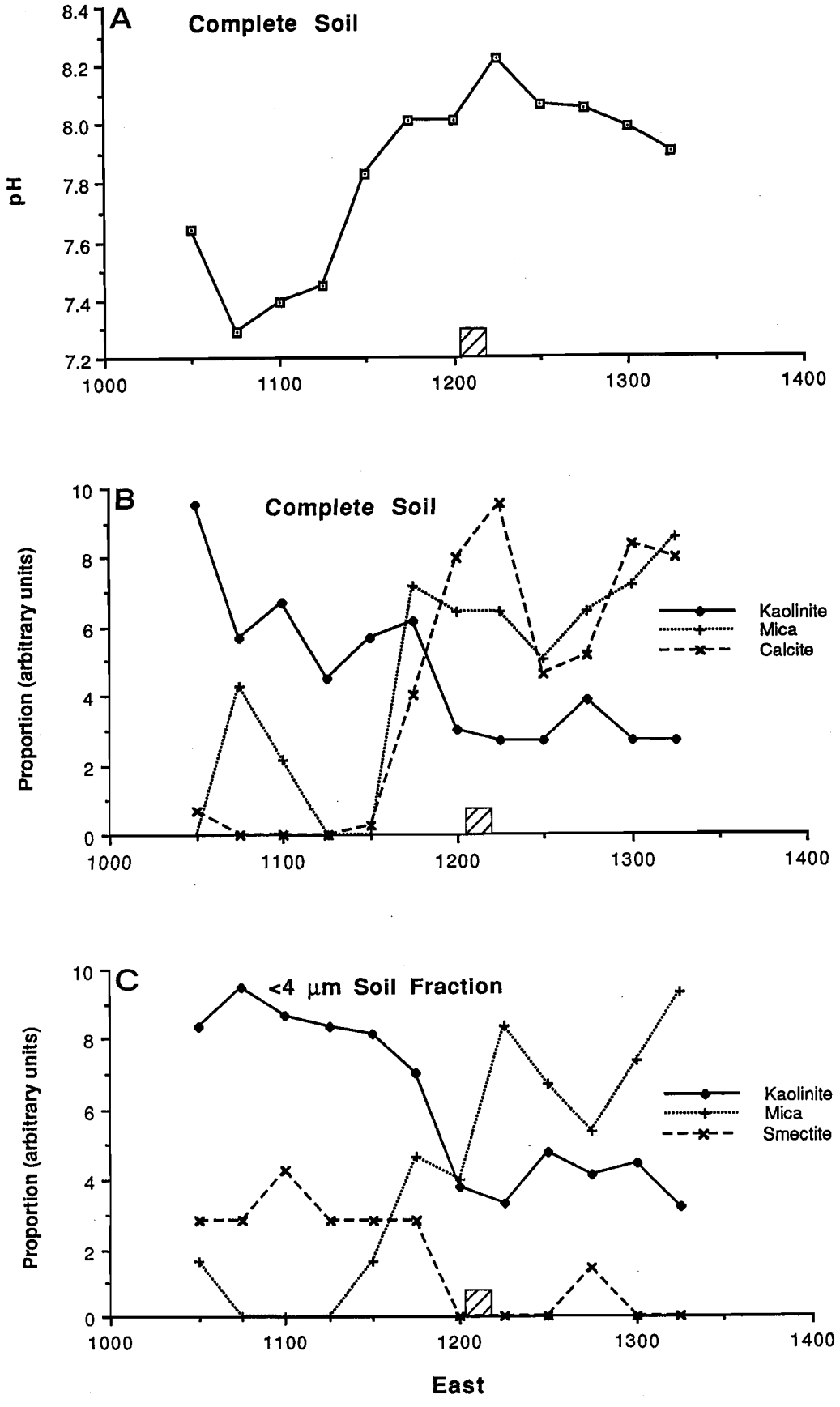

Figure 9. Mineralogy and pH of soil along traverse 1200mN.

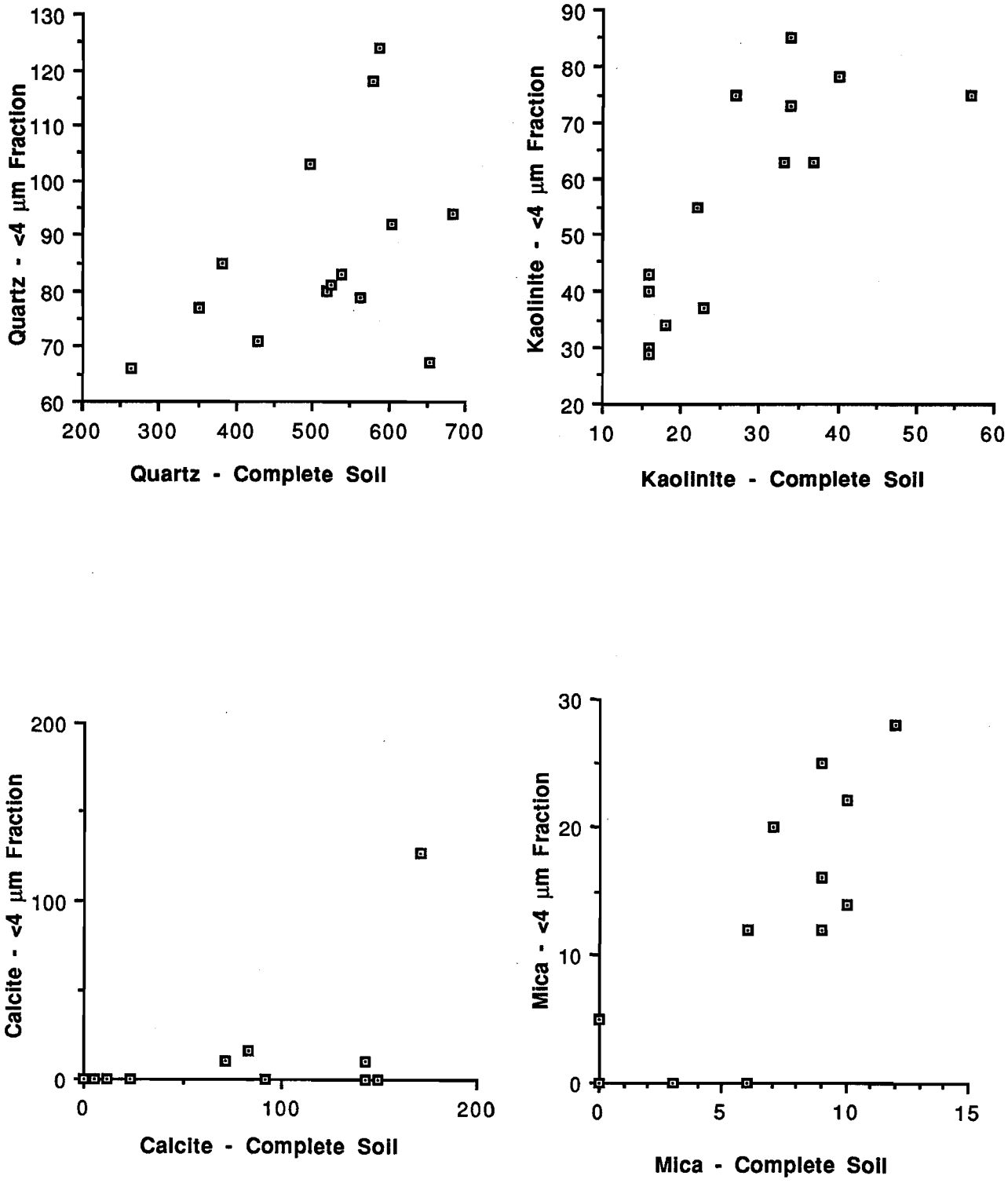

Figure 10. Effects of soil fractionation on soil mineralogy.

The silty, ferruginous <75 μm size fraction is dominant. This contrasts markedly with the much coarser, sandy soils examined at Beasley Creek (Robertson, 1990) which showed a mode in the 142-250 μm fraction. A binocular microscopic study of all size fractions indicated that iron-rich fragments were concentrated in the coarse and, to a lesser extent in the finest fractions, the intermediate fractions being relatively quartz-rich.

The relative mineralogical compositions of the various size fractions are compared in Figures 8C-E. The densities of the particles are shown in Figure 8B. The finest fractions (Figures 8C and D) are Fe oxide and clay rich (<4 μm, 20% by weight) with a slightly larger proportion of silt (4-75 μm, 33%). The intermediate fraction (75-710 μm; about 36%) consists largely of quartz sand (Figures 6F and 8E). The coarse fraction (>710 μm) is dense (Figures 8B and C) and consists mainly of ferruginous granules (LG201) and fragments of ferruginised saprolite (using the terminology and codes of Anand *et al.*,1989), with minor fragments of quartz and a trace of fresh tourmaline.

The very coarse fraction (>500 μm) is dominated by angular fragments of yellow-brown, deep red-brown and black nodules with minor fragments of vein quartz and a trace of tourmaline. The glossy, black, ferruginous fragments have partial nodular rims and are clearly fragments of larger nodules. They consist of hematite and maghemite, with no quartz or kaolinite. The red-brown fragments are less dense than the black, glossy fragments and consist of goethite, hematite, quartz and kaolinite. The yellow-brown fragments are less abundant than the other two types and consist of goethite-stained kaolinite and quartz. There are two quartz varieties; white, 'buck' quartz, and clear, well-crystalline, yellowish to glassy quartz, which is the most abundant. Most of this quartz is angular, though there are a very few rounded quartz grains.

In the 500-710 μm fraction, the proportion of quartz is greater and quartz increases progressively to become dominant in the 250-500 μm fraction (Figure 6H). There is a trace of angular, partly weathered cleavage fragments of microcline. Most of the quartz is angular and the amount of frosted, rounded quartz grains is very low (<1%) in the coarser fractions but this increases to 10-20% below 150 μm. The clay content is high to dominant below 75 μm (Figure 8D).

The trace amount of black tourmaline (schorl), which is significantly more abundant in sample LIC-58 (near mineralisation) than in LIC-53, is extremely fresh and angular (Figure 6H). It consists mostly of equant crystal fragments, many showing characteristic striations, parallel to the c axis, and triangular cross sections. There are also a few needle-like crystals and small bunches of parallel crystals.

The presence of much angular, glassy quartz, some showing crystal terminations, indicates little transport of most of the coarser fractions. This is supported by the angular cleavage fragments of microcline and the angular nature of the tourmaline. There is a significant increase in rounded, frosted, apparently aeolian grains (10-20%) below 150 μm. It is concluded that the coarse fractions of the soil are essentially residual and there is evidence only for minor, presumably aeolian, transport of the fine fractions. Most of the soil quartz probably was derived locally, from vein quartz, small pegmatites and quartz-tourmaline veinlets. This should be contrasted with the similar study at Beasley Creek where a considerable proportion of the finer fractions are aeolian and the quartz grains have a rounded, glossy appearance.

5.2 Soil Mineralogy

All complete soil samples and all samples of the <4 μm fraction were examined by XRD (Section 3.5). To compare trends in the mineralogy of the soil traverse, it was necessary to normalise the disparate ranges of the arbitrary (peak height) units of different minerals to a range

of 0-10. This does not represent the mode of the material but merely reflects variations in the content of each single mineral. This comparison is shown in Figure 9. Overall, the mineralogy of the soil was found to be more complex than that of Beasley Creek, the soil at Lights of Israel being a mixture of quartz, kaolinite, smectite, iron oxides (hematite, goethite, and minor maghemite), sericite, calcite, minor anatase and K-feldspar.

The presence of smectite in the complete soil is inferred from a slight bulge in the high XRD background at about 14Å; this becomes more distinctive in the <4 μm fraction, where it may be estimated only approximately. Semiquantitative estimates of the contents of quartz, kaolinite, calcite and sericite were made by measurement of the diffraction peak heights (see Section 3.6 and Table 1). Although iron oxides are also present as major components, semi-quantitative estimation of goethite and hematite was not possible, due to considerable peak overlap with kaolinite, quartz and sericite.

The effect that fractionation of the soil clays (<4 μm fraction) has had on the mineralogy is illustrated in Figure 10. The abundances of kaolinite and mica have been enhanced by the laboratory sedimentation process by a factor of two to three. Quartz has been significantly decreased by up to a factor of five but some separations were not as efficient as others, hence the scatter. The carbonate content has been significantly reduced in the <4 μm fraction. The occurrence of remnant carbonate in the <4 μm fraction may be generally correlated with abundant calcite in the complete soil but the remnant quantity is probably related not only to the original calcite abundance but also to the exposure period to acid during clay floculation, which was quite variable.

The whole soils have a progressive decrease in their kaolinite content and an increase in the abundance of mica (sericite) and calcite from west to east along the soil traverse (Figure 9B). The calcite content is closely followed by soil pH (Figure 9A). The increase in mica content may be related to a phyllic alteration halo around the mineralisation; whatever its cause, the elevated mica content has a significant influence on the geochemistry. The quartz and maghemite contents vary in a random manner.

The <4 μm fraction shows a similar trend of decreasing kaolinite and increasing mica (Figure 9C). In this fraction, smectite could be determined approximately and it also showed a decrease to the east, similar to kaolinite. Variations in the quartz abundance appears to be random.

6.0 LAG COMPOSITION

The wall-rock geology of mafic schists at the Lights of Israel Mine is relatively simple so the petrography of two samples of fresh rock are briefly described so that the fabrics of their weathered and ferruginised equivalents may be better understood. The petrography of the coarse lag is given in detail in Appendix 16 and in summary here. The lag consists largely of ferruginised saprolite.

6.1 Fresh Rock Mineralogy and Petrography

Sample LOI-112 from a depth of about 45 m (1180 mN, 1150 mE, 412 R.L.) consists of a slightly gneissic mass of quartz, plagioclase and actinolitic amphibole, with minor opaques (magnetite or ilmenite and some pyrite) and a trace of sphene. The feldspar is granular and has sutured margins. The amphibole is subhedral to euhedral and shows wedge-shaped cross sections and acicular, longitudinal sections, where it defines a penetrative gneissosity. Some zones, probably marking a non-penetrative cleavage, are marked by granules of epidote and

FIGURE 11
Petrography of Ferruginous Granules

A. A subrounded fragment of slightly porous secondary hematitic goethite (Gh), set in spongy goethite (Gt). Specimen LOI-08. Co-ordinates 1175 mE; 1200 mN.

B. A well-preserved, pseudomorphed layer silicate fabric (Ss), probably after saprolitic clays, set in goethite (Gt). Part of a lag fragment. Specimen LOI-10. Co-ordinates 1225 mE; 1200 mN.

C. Pseudomorphed layer silicates (Sc), probably smectites, and a relict tourmaline (Tm). The basal parting of the tourmaline has been penetrated by hematitic goethite (Gh), otherwise it is fresh. Specimen LIC-53. Co-ordinates 1100 mE; 1200 mN.

D. A less well-preserved layer silicate fabric (Ls) which has been partly dissolved, leaving small voids (V). These have been coated internally with colloform goethite (Gc). Specimen LOI-10. Co-ordinates 1225 mE; 1200 mN.

E. A secondary fabric of bright, stellate hematite, which may, in part, be pseudomorphing the rhombohedral cleavage of primary carbonate. Specimen LOI-13. Co-ordinates 1300 mE; 1200 mN.

F. Bright goethitic boxwork after pyrite pyritohedra (Pg)- presumably a gossan fragment. This lag sample is from above the orebody subcrop and assays 0.726 g/t Au. Specimen LOI-10. Co-ordinates 1225 mE; 1200 mN.

G. A secondary deposit of successive, thin layers of goethite (Gc) with a cuspate fabric in a void in spongy goethite. Specimen LOI-04. Co-ordinates 1075 mE; 1200 mN.

H. Perfect goethite pseudomorphs after kaolinite accordion structures (Ga). This is not a primary fabric but a saprolite or pedolithic authigenic clay structure. Specimen LOI-06. Co-ordinates 1125 mE; 1200 mN.

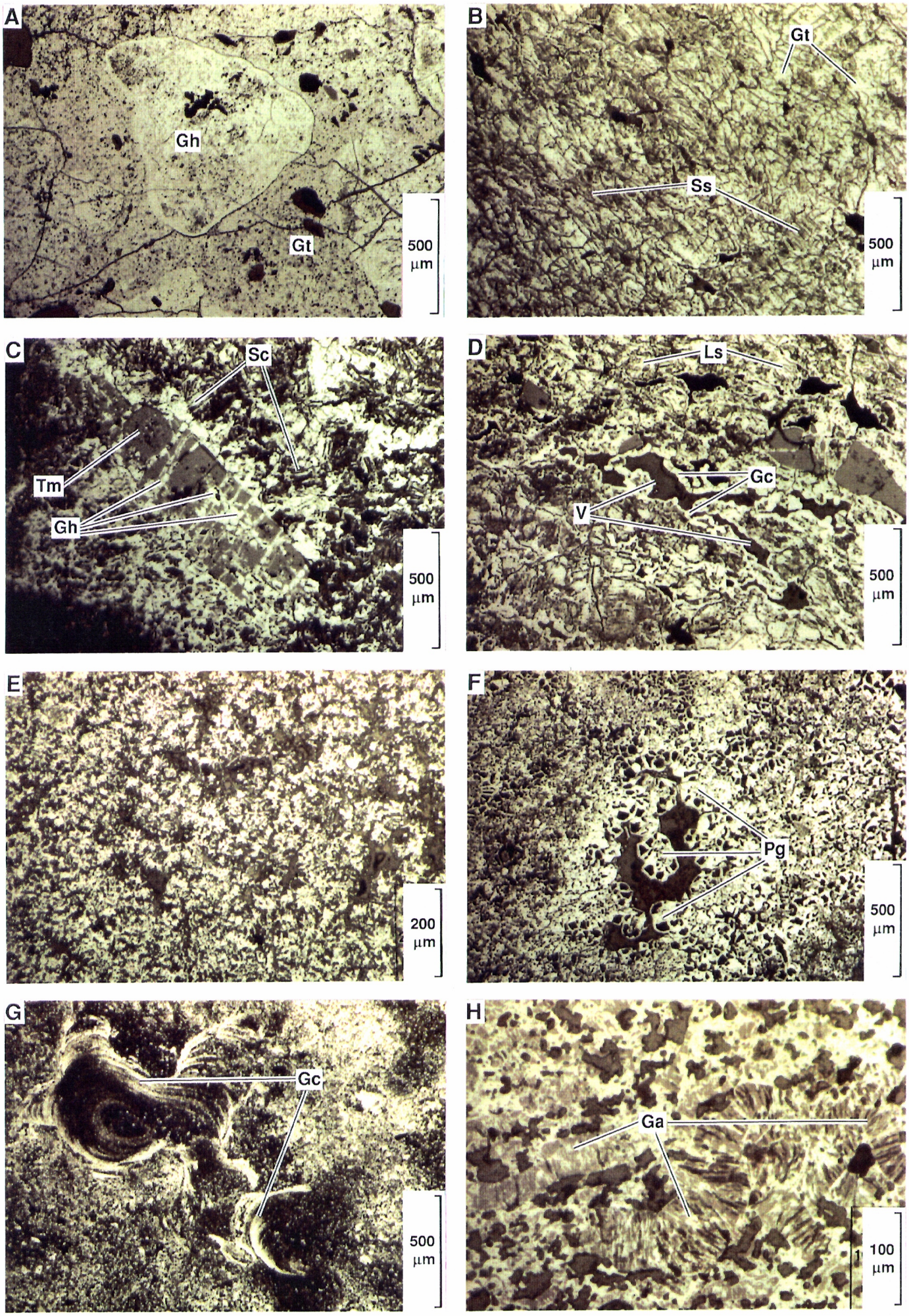
A
Gh
Gt
500 µm
B
Gt
Ss
500 µm
C
Sc
Tm
Gh
500 µm
D
Ls
Gc
V
500 µm
E
200 µm
F
Pg
500 µm
G
Gc
500 µm
H
Ga
100 µm

flakes of chlorite. In one part of the slide, the margins of some grains, chiefly amphibole, are stained with goethite, although the accompanying pyrite is fresh. The metamorphic grade is amphibolite facies with some retrogression to greenschist facies, accompanied by inhomogeneous strain.

Sample LOI-111, from a depth of about 43 m (1110 mN, 1100 mE, 414 R.L.), is similar to sample LOI-112 but it is very fine-grained (30 μm) and it lacks the later cleavage and retrogression. It consists of granular quartz and plagioclase and granular to stumpy crystals of actinolitic amphibole, with minor magnetite or ilmenite and some biotite. No sulphides were visible. The metamorphic grade is amphibolite facies with no significant retrogression and no carbonation or sulphide mineralisation.

6.2 Lag Fabrics

Internal fabrics are revealed by polished sections. These fabrics commonly vary greatly at any particular site, due to mechanical dispersion of lag particles and to varying states of fabric preservation. It is therefore essential to examine several lag fragments at a site to detect fabrics diagnostic of the underlying rock. Many of the elements of the lag fabric (secondary goethite, its dehydration product, hematite, and pseudomorphs after saprolitic clays) described at Beasley Creek (Robertson, 1989) are also seen here, with minor differences.

Fine-grained, dark-grey to dark red-brown, slightly laminated and porous, goethitic fragments are pieces of *ferruginised saprolite* and contain preserved but pseudomorphed layer silicate fabrics. These fingerprint layer-silicate fabrics (after clay) are completely surrounded and separated by bright goethite and hematitic goethite (Figure 11B, C and D). Close to the subcrop of the mineralisation, some pseudomorphs after fine-grained pyrite (Figure 11F) show a minor *gossan* component in the lag. Dark grey to honey-brown, very fine-grained and dense fragments contain secondary hematitic colloform fabrics (Figure 11D), void-filling, goethitic, cuspate fabrics (Figure 11G) and cracks occur in hematite (due to dehydration of goethite). Included in some are relict grains of tourmaline, which are still fresh and sharp, but iron oxides have penetrated the basal parting (Figure 11C). Some contain weakly-preserved layer silicate fabrics which have been blurred (Figure 11C) by the replacement of goethite by hematite; others are stellate (Figure 11E), possibly after pre-existing carbonates. *Accordion structures* (Figure 11H) indicate authigenic recrystallisation of kaolinite and lozenge shaped crystals of hematite suggest several cycles of iron oxide recrystallisation. Red-brown, *composite nodules* of hematitic clay are formed around earlier goethite and hematite fragments and represent duricrust remnants. Some of the ferruginous clays show internal pisolitic structures and are generally honeycombed with vermiform voids and solution channels, many of which are lined (Figure 11D) and even filled with secondary goethite. Some nodules of hematitic clay have partial rims of layered goethite. Breccias of the first two types are cemented by spongy secondary goethite (Figure 11A) and some contain inclusions of quartz.

Thus, there is a wide variety of primary fabrics (tourmaline and pyrite pseudomorphs) saprolitic fabrics (fingerprint layer silicate fabrics in varied states of preservation), authigenic pedolithic fabrics (accordion structures) and void-filling fabrics (colloform fabrics, cuspate fabrics). The fingerprint fabrics appear to be typical of mafic rocks (see Robertson, 1989). These varied fabrics indicate preservation of relics of parts of the whole weathered profile by ferruginisation and underline the relevance of lag petrography to bedrock identification.

TABLE 3A

SOIL BACKGROUND GEOCHEMISTRY

COMPLETE SOIL

Lib No	SiO2	Al2O3	Fe2O3	MgO	CaO	Na2O	K2O	TiO2	P2O5	S	Ag	As	Au	Ba	Bi	Cd	Ce	Ce	Co	
	%	%	%	%	%	%	%	%	%	%	ppm	ppm	ppb	ppm	ppm	ppm	ppm	ppm	ppm	
08-1577	57.18	13.70	14.09	1.37	0.59	0.65	0.92	0.88	0.049	0.021	0.31	5.91	5	210	0.23	0.10	36	37	41	
08-1578	48.21	12.05	28.22	0.63	0.48	0.18	0.41	1.43	0.041	0.019	0.22	8.27	9	296	0.18	0.10	21	27	26	
Mean	52.70	12.88	21.16	1.00	0.54	0.42	0.67	1.16	0.045	0.020	0.27	7.09	7	253	0.21	0.10	29	32	33	
Lib No	**Cr**	**Cu**	**Ga**	**Ge**	**In**	**La**	**Mn**	**Mo**	**Nb**	**Ni**	**Pb**	**Rb**	**Sb**	**Sn**	**Sr**	**V**	**W**	**Y**	**Zn**	**Zr**
	ppm	ppm	ppm	ppm	ppm	ppm	ppm	ppm	ppm	ppm	ppm	ppm	ppm	ppm	ppm	ppm	ppm	ppm	ppm	ppm
08-1577	242	104	20	1	0.09	20.6	1674	3.5	10	108	7	56	0.5	1.44	55	285	1.8	22	99	129
08-1578	490	80	24	0	0.11	11.5	760	3.3	7	102	7	21	0.9	1.14	54	538	1.6	13	60	158
Mean	366	92	22	1	0.10	16.0	1217	3.4	9	105	7	39	0.7	1.29	55	412	1.7	18	80	144

>600 μm FRACTION

Lib No	SiO2	Al2O3	Fe2O3	MgO	CaO	Na2O	K2O	TiO2	P2O5	S	Ag	As	Au	Ba	Bi	Cd	Ce	Ce	Co	
	%	%	%	%	%	%	%	%	%	%	ppm	ppm	ppb	ppm	ppm	ppm	ppm	ppm	ppm	
08-1593	37.95	6.21	51.36	0.25	0.29	0.11	0.06	1.24	0.072	0.011	0.12	13.45	90	157	0.39	0.23	60	86	43	
08-1594	26.44	10.25	56.12	0.28	0.36	0.09	0.06	1.84	0.064	0.014	0.48	18.29	5	375	0.28	0.11	20	63	34	
Mean	32.20	8.23	53.74	0.27	0.33	0.10	0.06	1.54	0.068	0.013	0.30	15.87	48	266	0.34	0.17	40	75	38	
Lib No	**Cr**	**Cu**	**Ga**	**Ge**	**In**	**La**	**Mn**	**Mo**	**Nb**	**Ni**	**Pb**	**Rb**	**Sb**	**Sn**	**Sr**	**V**	**W**	**Y**	**Zn**	**Zr**
	ppm	ppm	ppm	ppm	ppm	ppm	ppm	ppm	ppm	ppm	ppm	ppm	ppm	ppm	ppm	ppm	ppm	ppm	ppm	ppm
08-1593	522	116	23	1	0.18	46.7	2590	4.7	6	139	23	1	1.2	0.75	43	976	4.7	34	149	111
08-1594	908	108	32	0	0.19	14.2	747	4.9	5	136	10	1	1.9	1.33	44	1141	2.0	14	115	143
Mean	715	112	28	1	0.19	30.4	1669	4.8	6	138	17	1	1.6	1.04	44	1059	3.4	24	132	127

<75 μm FRACTION

Lib No	SiO2	Al2O3	Fe2O3	MgO	CaO	Na2O	K2O	TiO2	P2O5	S	Ag	As	Au	Ba	Bi	Cd	Ce	Ce	Co	
	%	%	%	%	%	%	%	%	%	%	ppm	ppm	ppb	ppm	ppm	ppm	ppm	ppm	ppm	
08-1609	51.23	19.45	11.61	1.99	0.77	0.39	1.32	1.13	0.058	0.010	0.14	5.72	8	229	0.14	0.13	42	47	45	
08-1610	55.31	16.04	12.77	1.08	0.81	0.48	0.77	1.65	0.037	0.012	0.18	3.91	12	254	0.18	0.05	29	42	33	
Mean	53.27	17.75	12.19	1.54	0.79	0.44	1.05	1.39	0.048	0.011	0.16	4.82	10	242	0.16	0.09	35	45	39	
Lib No	**Cr**	**Cu**	**Ga**	**Ge**	**In**	**La**	**Mn**	**Mo**	**Nb**	**Ni**	**Pb**	**Rb**	**Sb**	**Sn**	**Sr**	**V**	**W**	**Y**	**Zn**	**Zr**
	ppm	ppm	ppm	ppm	ppm	ppm	ppm	ppm	ppm	ppm	ppm	ppm	ppm	ppm	ppm	ppm	ppm	ppm	ppm	ppm
08-1609	251	127	25	1	0.11	21.4	1599	3.7	11	129	11	82	0.5	1.32	65	260	1.9	27	126	207
08-1610	319	82	21	1	0.10	14.6	1089	3.1	11	109	6	38	0.5	0.88	73	234	2.0	21	59	268
Mean	285	105	23	1	0.11	18.0	1344	3.4	11	119	9	60	0.5	1.10	69	247	1.9	24	93	238

<4 μm FRACTION

Lib No	SiO2	Al2O3	Fe2O3	MgO	CaO	Na2O	K2O	TiO2	P2O5	S	Ag	As	Au	Ba	Bi	Cd	Ce	Ce	Co	
	%	%	%	%	%	%	%	%	%	%	ppm	ppm	ppb	ppm	ppm	ppm	ppm	ppm	ppm	
08-1625	46.10	22.04	13.38	2.21	0.66	0.43	1.29	1.03	0.070	0.012	0.20	5.74	24	157	0.28	0.05	45	55	37	
08-1626	45.90	20.54	14.04	1.44	0.73	0.12	0.56	0.75	0.043	0.005	0.22	3.64	12	176	0.17	0.13	12	29	19	
Mean	46.00	21.29	13.71	1.83	0.70	0.28	0.93	0.89	0.057	0.009	0.21	4.69	18	167	0.23	0.09	29	42	28	
Lib No	**Cr**	**Cu**	**Ga**	**Ge**	**In**	**La**	**Mn**	**Mo**	**Nb**	**Ni**	**Pb**	**Rb**	**Sb**	**Sn**	**Sr**	**V**	**W**	**Y**	**Zn**	**Zr**
	ppm	ppm	ppm	ppm	ppm	ppm	ppm	ppm	ppm	ppm	ppm	ppm	ppm	ppm	ppm	ppm	ppm	ppm	ppm	ppm
08-1625	227	145	29	2	0.13	23.0	1286	1.8	12	137	9	82	0.5	1.82	54	299	0.9	29	140	146
08-1626	220	98	27	1	0.10	9.0	633	1.3	6	128	3	35	0.4	1.36	64	237	0.6	15	68	105
Mean	223	122	28	2	0.12	16.0	960	1.6	9	133	6	59	0.4	1.59	59	268	0.8	22	104	126

TABLE 3B

LAG BACKGROUND GEOCHEMISTRY

COARSE LAG															
No	SiO2	Al2O3	Fe2O3	MgO	CaO	TiO2	As	Au	Ba	Be	Ce	Co	Cr	Cu	Ga
	%	%	%	%	%	%	ppm	ppb	ppm	ppm	ppm	ppm	ppm	ppm	ppm
08 - 406	10.80	3.52	71.49	0.33	0.76	0.70	13.0	5.7	266	0	44.3	177	117	234	7
08 - 407	8.26	4.62	70.34	0.28	0.30	5.08	10.8	6.4	184	0	11.6	47	433	61	33
Mean	9.53	4.07	70.92	0.31	0.53	2.89	11.9	6.1	225	0	28.0	112	275	148	20
No	Ge	La	Mn	Mo	Nb	Ni	Pb	Rb	Sb	Sr	V	W	Y	Zn	Zr
	ppm	ppm	ppm	ppm	ppm	ppm	ppm	ppm	ppm	ppm	ppm	ppm	ppm	ppm	ppm
08 - 406	0	36.1	7034	5.2	0	233	33	4	0.48	64	1094	2.3	48	367	40
08 - 407	0	5.7	934	4.6	5	90	14	2	1.16	40	1882	5.5	11	101	160
Mean	0	20.9	3984	4.9	3	162	24	3	0.82	52	1488	3.9	30	234	100
FINE LAG															
No	SiO2	Al2O3	Fe2O3	MgO	CaO	TiO2	As	Au	Ba	Be	Ce	Co	Cr	Cu	Ga
	%	%	%	%	%	%	ppm	ppb	ppm	ppm	ppm	ppm	ppm	ppm	ppm
08 - 408	28.00	6.33	53.47	0.23	0.23	1.68	15.1	6.7	91	0	49.8	41	562	104	26
08 - 409	16.20	10.40	58.33	0.26	0.26	2.64	17.2	5.3	191	0	17.5	29	834	84	33
Mean	22.10	8.37	55.90	0.25	0.25	2.16	16.2	6.0	141	0	33.7	35	698	94	30
No	Ge	La	Mn	Mo	Nb	Ni	Pb	Rb	Sb	Sr	V	W	Y	Zn	Zr
	ppm	ppm	ppm	ppm	ppm	ppm	ppm	ppm	ppm	ppm	ppm	ppm	ppm	ppm	ppm
08 - 408	2	39.7	2473	5.0	0	119	34	4	1.59	26	1474	4.3	25	120	108
08 - 409	2	12.3	833	4.8	4	118	20	0	1.40	40	1770	3.0	10	68	130
Mean	2	26.0	1653	4.9	2	119	27	2	1.50	33	1622	3.7	18	94	119
FINE NON-MAGNETIC LAG															
No	SiO2	Al2O3	Fe2O3	MgO	CaO	TiO2	As	Au	Ba	Be	Ce	Co	Cr	Cu	Ga
	%	%	%	%	%	%	ppm	ppb	ppm	ppm	ppm	ppm	ppm	ppm	ppm
08 - 410	45.60	6.80	36.74	0.18	0.17	1.09	14.1	4.9	66	0	35.9	23	425	103	19
08 - 411	21.20	12.30	52.04	0.29	0.27	2.35	16.3	6.7	183	0	14.6	33	818	100	33
Mean	33.40	9.55	44.39	0.24	0.22	1.72	15.2	5.8	125	0	25.3	28	622	102	26
No	Ge	La	Mn	Mo	Nb	Ni	Pb	Rb	Sb	Sr	V	W	Y	Zn	Zr
	ppm	ppm	ppm	ppm	ppm	ppm	ppm	ppm	ppm	ppm	ppm	ppm	ppm	ppm	ppm
08 - 410	0	34.7	1482	4.4	1	73	23	2	1.24	22	1118	2.6	23	67	78
08 - 411	0	13.1	762	4.8	0	107	33	2	1.42	34	1633	3.2	12	72	112
Mean	0	23.9	1122	4.6	1	90	28	2	1.33	28	1376	2.9	18	70	95
FINE MAGNETIC LAG															
No	SiO2	Al2O3	Fe2O3	MgO	CaO	TiO2	As	Au	Ba	Be	Ce	Co	Cr	Cu	Ga
	%	%	%	%	%	%	ppm	ppb	ppm	ppm	ppm	ppm	ppm	ppm	ppm
08 - 412	7.96	6.03	73.20	0.31	0.29	2.50	16.8	6.0	124	0	67.8	66	746	93	30
08 - 413	9.00	8.26	69.34	0.27	0.32	3.36	20.3	6.0	250	0	21.8	27	1076	56	43
Mean	8.48	7.15	71.27	0.29	0.31	2.93	18.6	6.0	187	0	44.8	47	911	75	37
No	Ge	La	Mn	Mo	Nb	Ni	Pb	Rb	Sb	Sr	V	W	Y	Zn	Zr
	ppm	ppm	ppm	ppm	ppm	ppm	ppm	ppm	ppm	ppm	ppm	ppm	ppm	ppm	ppm
08 - 412	2	48.0	3492	5.5	1	173	45	5	2.12	33	1912	8.4	30	177	140
08 - 413	0	14.3	959	5.4	4	88	43	3	2.31	41	1964	3.5	12	49	154
Mean	1	31.2	2226	5.5	3	131	44	4	2.22	37	1938	6.0	21	113	147

7.0 GEOCHEMISTRY

The composition of the complete soil, the soil size fractions, the lag and its components are discussed systematically so that the performance of each medium and its components may be compared. The data are displayed as transects in Appendix 3, are tabulated in full in Appendices 1 and 2 and are available in a data disc as Appendix 21. Histograms are available in Appendices 4-11.

Inter-element correlations have been investigated by means of correlation matrices (Appendix 12). Prior to calculating the correlations, the data were normalised, using the Box-Cox generalised power transformation (Appendix 17). For 14 samples, any correlation over 0.458 is statistically significant at the 95% confidence limit, over 0.612 is significant at the 99% confidence limit and over 0.780 is significant at the 99.9% confidence limit. Such correlations have been highlighted in Appendix 12. The inter-element correlations may be used to provide a hint as to the mineralogical siting of some trace elements. Similar techniques of analysis and lag and soil fractionation have been used at Beasley Creek, so direct comparisons may be made with a similar orientation study in a more arid area (Robertson, 1989; 1990).

7.1 Geochemical Background

Establishing geochemical background is an important function of an orientation survey. The soil and lag survey did not extend beyond 1325 mE and the survey was terminated by the mine lease to the west. It is probable that the regional geochemical background was not reached for some elements in this rather limited survey. To test this, two soil and two lag samples were collected along strike, 825 m and 500 m to the north and south respectively of the pit centre, remote from mineralisation (Figure 5) and were used to estimate the 'regional' background. This regional background data are given in Tables 3A and B. A number of elements, notably S, As, Au, Cd, Cu and W appear to have substantially higher abundances in the lag and soil survey over the site of the pit (local background) than was found in the regional background (Table 4). Such elements may be potential pathfinders.

TABLE 4
Elements More Abundant In Local Than Regional Background

	Coarse Lag	Fine Lag	Fine Mag	Fine NonMag	Whole Soil	>600 µm	<75 µm	<4 µm
S	-	-	-	-	√	√	√	√
As	√	√	?	√	x	√	?	√
Au	√	√	√	√	√	√	√	√
Cd	-	-	-	-	√	√	?	?
Cu	x	√	?	√	√	√	x	√
Mn	x	√	x	√	x	√	x	x
Mo	x	x	√	√	x	x	x	√
Pb	x	√	?	√	?	√	x	?
Sb	√	x	√	√	x	?	x	x
W	√	√	√	√	?	x	√	√
Zn	x	√	x	√	x	x	x	x

√ = yes; x = no; ? = possibly

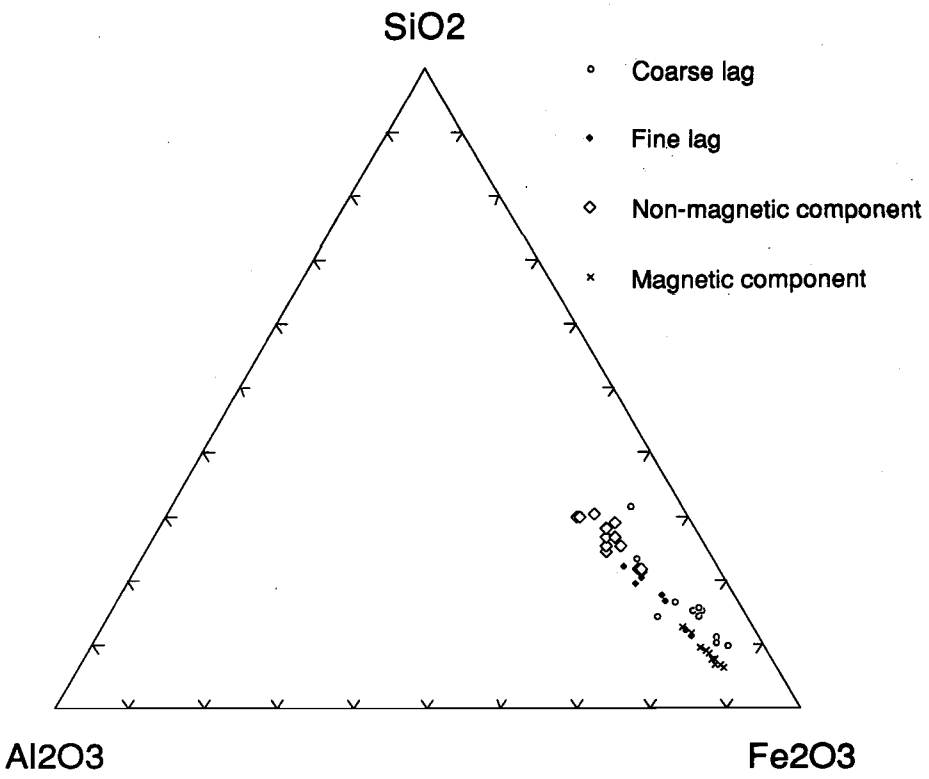

Figure 12A. Ternary Si-Al-Fe plot of lag and its components.

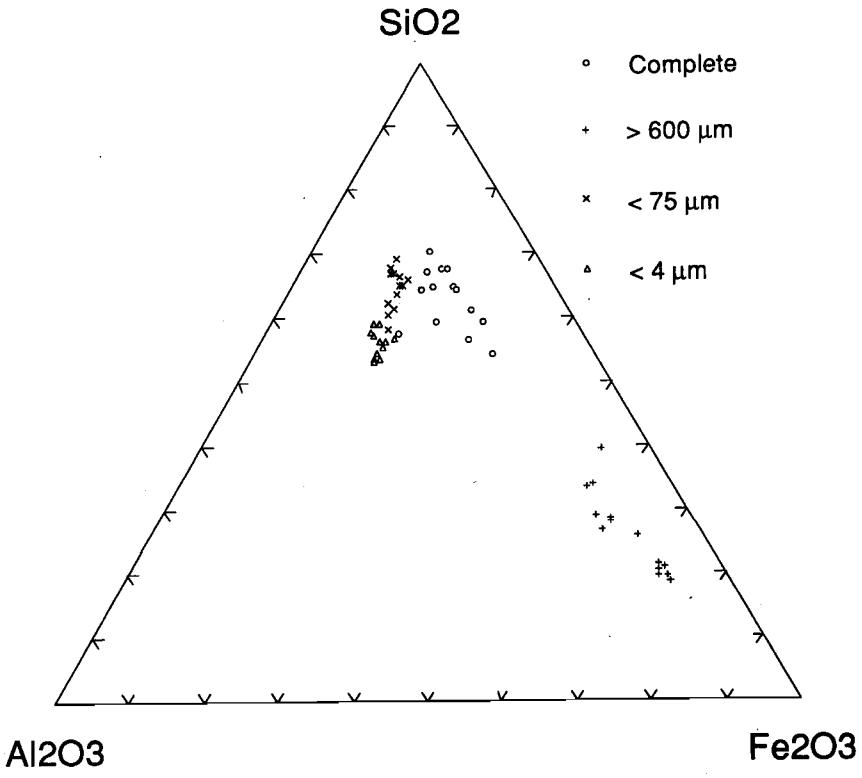

Figure 12B. Ternary Si-Al-Fe plot of soil and its fractions.

7.2 Major and Associated Trace Elements (Si, Al, Fe, Ga, V, In, Ge)

Silicon and Aluminium. The magnetic component of the fine lag is the least siliceous and its non-magnetic component the most siliceous, reflecting the Fe oxide content and displacement of Si by Fe oxides. The background coarse lag samples have very low Si abundances. The complete soil and the quartz-rich <75 μm fraction are the most siliceous and the ferruginous >600 μm fraction has the least silica. The Si content reflects the abundance of quartz in the samples and does not appear to be related to mineralisation. The fine lag and its dominant non-magnetic component are the most aluminous (10-12%) and their Al abundances decrease towards the east, reflecting the decrease in kaolinite observed in the soil (Section 7). The magnetic component (due to maghemite) of both the fine and coarse lag is the least aluminous (4-8%) and is relatively constant in Al content across the traverse. The aluminous parts of the soils show a similar trend to the lag (decreasing Al to the east), reflecting the decreased kaolinite content (Section 7) with the clay-rich, fine fractions being the most aluminous and the ferruginous >600 μm fraction the least. This latter fraction has a relatively constant Al content (10% Al_2O_3). Apart from the obvious increase in Fe, the decline in soil Al abundance to the east reflects a corresponding increase in Mg and Ca, which occur as soil carbonates. This relationship is strong in the <4 μm and <75 μm fractions but does not occur in the ferruginous >600 μm fraction.

Iron. All the lag components are very ferruginous (47-73% Fe_2O_3), the magnetic component of the fine lag being particularly ferruginous and its non-magnetic part the least. The >600 μm fraction of the soils is the most ferruginous, with a composition analogous to the lag; the sandy <75 μm and clay-rich <4 μm fractions are Fe-poor. There appears to be a slight increase in the Fe content of the lag and the >600 μm soil fraction to the east, in the vicinity of the mineralisation.

Silicon-Aluminium-Iron Relationship. The Si-Al-Fe relationships of the lag and soil and their components are shown in the ternary diagrams of Figure 12. These relationships are very similar to those from Beasley Creek (Robertson, 1989; 1990). The lag shows a trend from the most ferruginous magnetic component to the less ferruginous non-magnetic component, at an Al/Si ratio which is more siliceous than would be expected from variation in the content of kaolinite. Similarly, the trend of the >600 μm soil fraction is more siliceous than would be expected from variation in the kaolinite content. This probably reflects minor quartz chips and/or cryptocrystalline silica included with the lag.

Gallium. There is a moderate to strong correlation between Ga and Al in the fine soil fractions, indicating Ga substitution in kaolinite; Ga is most abundant (30-40 ppm) in the ferruginous, coarse soil fraction and particularly so (45-60 ppm) in the magnetic component of the fine lag, indicating Ga association with Fe oxides (there is also a high Ga correlation in this component with Ti, V, Sb and Zr). This is similar to the findings at Beasley Creek (Robertson, 1989; 1990). The Ga content in the coarse soil fraction at Lights of Israel increases to the east of the drainage and over the deposit but this is probably related to Fe oxides and not to mineralisation. Gallium is closely associated with Al and, like Al, it is concentrated in the products of lateritic weathering. However, it is more mobile than Al, so the Ga/Al ratio tends to decrease slightly where weathering is most intense. Gallium may also be associated with magnetic iron minerals (Lavrenchuk and Tenyakov, 1962,1963 ; Burton and Culkin, 1978).

Vanadium. The V abundance is greater in lag than soil, clearly related to the greater relative Fe contents. There is no V anomaly marking the ore position. Vanadium-bearing minerals, (muscovite, magnetite, ilmenite and mafic minerals) are relatively easily weathered and V is mobile under a variety of oxidising, acid to alkaline conditions. Hence, V is strongly correlated

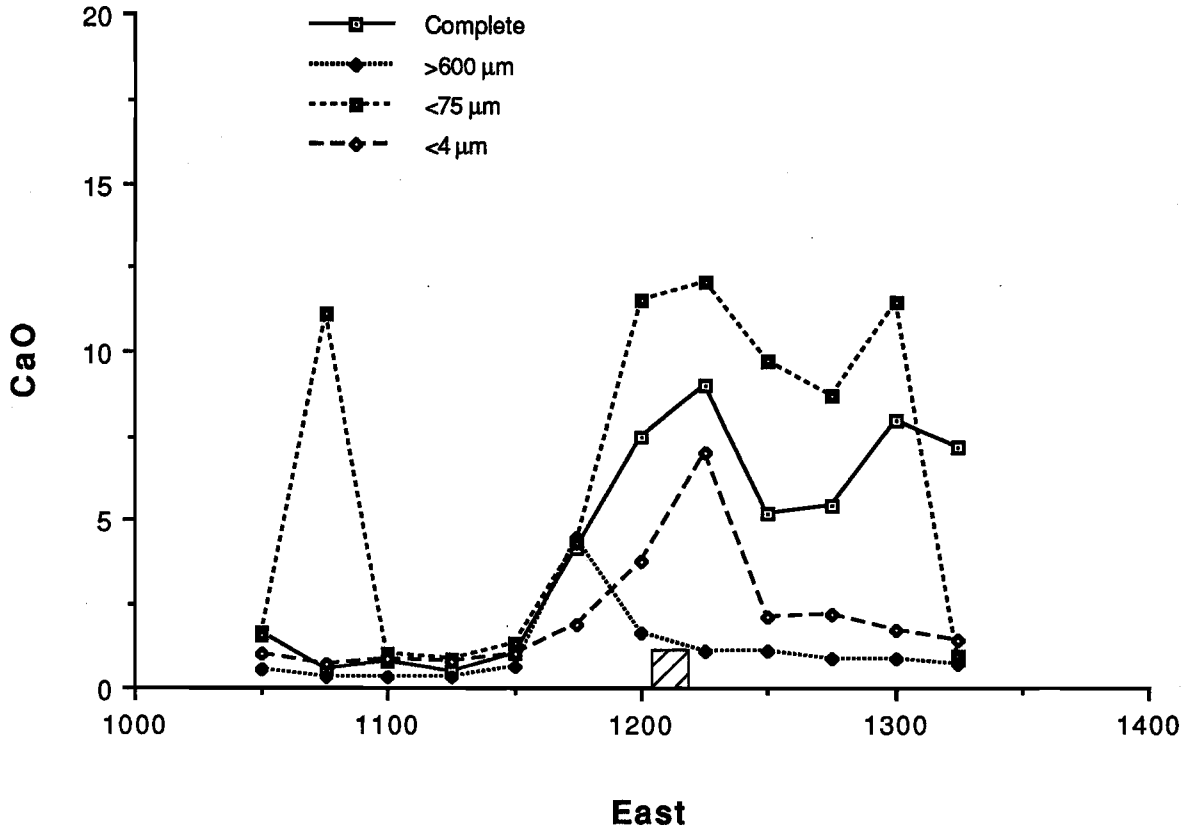

Figure 13A. Lime content of traverse, showing surficial soil and its fractions.

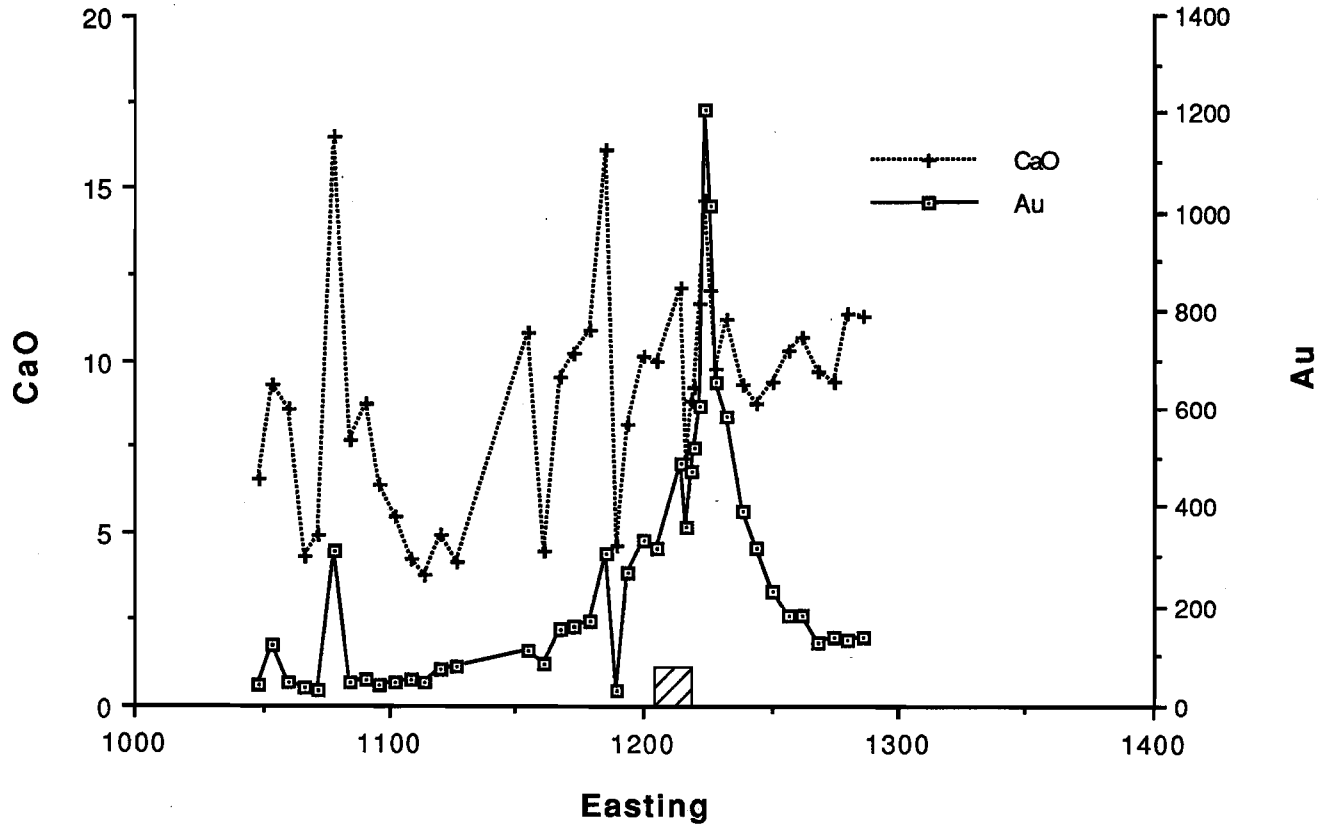

Figure 13B. Lime and Au content of Ditchwitch traverse 1200 mN.

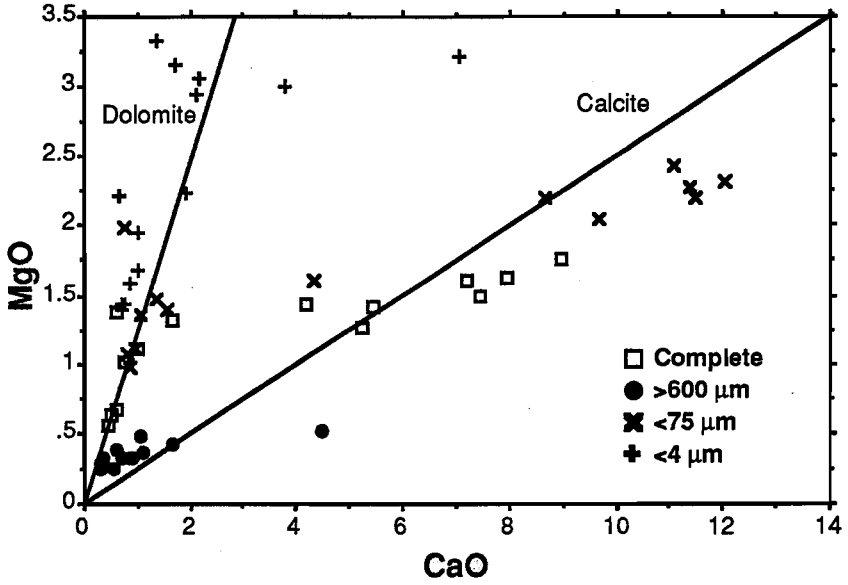

Figure 14A. Mg and Ca relationships of soil and its fractions.

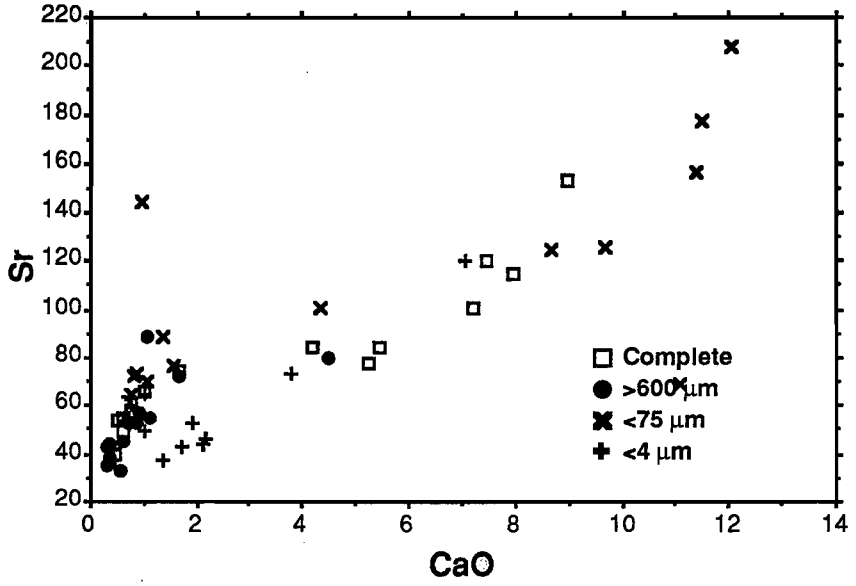

Figure 14B. Sr and Ca relationships of soil and its fractions.

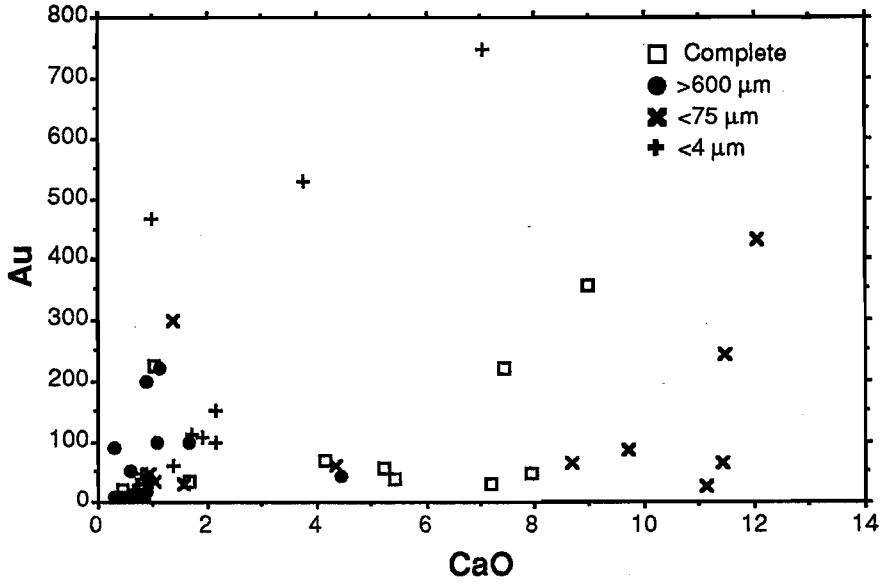

Figure 14C. Au and Ca relationships of soil and its fractions.

with Fe, Ti, Ga and Zr in almost all media, which suggests that it was adsorbed by, or was co-precipitated with, the Fe oxyhydroxides.

Germanium. Almost all the Ge data from the lag and soil lie below the XRF detection limit of 3 ppm and display analytical noise. An improved analytical method, such as ICP-MS with a lower detection limit (0.5), may be required for meaningful Ge results.

7.3 Alkaline Earth Elements (Mg, Ca, Sr and Ba)

Soils with a high Ca abundance (>2.5% CaO) are characterised by a high pH (7.9-8.2; Figure 9A) and the presence of carbonate minerals (Section 5; Figure 9B). Such pedogenic carbonates are typical of soils south of the Menzies Line, where a strong association between Au and soil carbonate has been demonstrated (Lintern, 1989; Lintern *et al.*, 1990; Lintern and Scott, 1990; Gray *et al.*, 1990).

Calcium and Magnesium. There is a marked increase in soil Mg and Ca in the whole soil and in the fine soil fraction east of the stream, which reach a peak over the mineralisation and decline further east (Figure 13A). The >600 μm soil fraction does not show this peak for Mg and only weakly for Ca. The strongest Ca peaks occur in the <75 μm fraction and in the complete soil, indicating that soil carbonate is relatively fine-grained here but is mostly greater than clay-sized particles. The <4 μm fraction retains a little soil carbonate (Section 7), despite acidification during clay separation.

There are strong correlations between Ca and Mg in the soil, the strongest occurring in the complete soil, the >600 μm and <75 μm fractions; the <4 μm fraction has the least. The <75 μm fraction has a Ca/Mg ratio of 4.0, indicating a slightly dolomitic calcite composition (Figure 14A). The <4 μm fraction is much more Mg rich (CaO/MgO = 0.83), corresponding to dolomite, which would be less soluble during clay flocculation. Strontium is strongly correlated with Ca (Figure 14B) but less so with Mg. There is a strong correlation of Ca with Au (Figure 14C) in the finest soil fractions and in the lag, discussed below. Potassium and Rb in the soil are correlated with Mg but not with Ca, probably reflecting sericite. The rare earth elements, Ce and La, show limited correlation with Mg and Ca in both media. Apart from a single point peak in the coarse lag, probably due to an included Mg-rich mineral, there is no Mg response in the lag; Ca shows a weak response in all but the magnetic lag component, presumably due to small carbonate fragments and chips.

Variations in the soil Ca content are related to sampling depth. The soil samples taken for this study were from the top 250 mm. Data from a later ditchwitch sampling traverse (approx 1 m) are shown in Figure 13B for comparison. If sampled deeply enough, the soils to the west of the drainage have a much higher Ca background (9% CaO) than shown by the shallow soil sampling. The Ca anomaly over the mineralisation, as shown by the near-surface sampling, is an artifact of sampling depth.

Strontium. There is a significant apparent Sr peak associated with the mineralisation in all high pH soil fractions, though least so in the >600 μm fraction. The ditchwitch sample traverse showed that the low Sr background west of the drainage is actually much higher and that sampling depth is critical.

There is no such peak in any of the lag media. The Sr regional background is significantly lower than the local Sr background. In almost all media there is a strong correlation of Sr with Ca, and with Au in the fine soil fractions. In addition to Ca in the lag, Sr is also correlated with Mg and, in some, with Ba. Clearly Sr is contained in soil carbonates and, less so in lag carbonates, which are in part dolomitic.

Barium. The fine lag and all its components show an anomaly in Ba in the vicinity of the mineralisation from a background of 120-150 to over 300 ppm. This is largely confirmed by the >600 μm soil fraction but not by the fine soil fractions. The coarse lag shows a reverse trend. This Ba anomaly in the ferruginous media is not nearly as strong as that encountered at Beasley Creek (1800-2500 ppm) where it also occurs in the lag and ferruginous, coarse soil fraction. In the soil, Ba is correlated with Ti in all but the <75 μm fraction, with Ga, Sb, Sr and Zr in the ferruginous component and with Fe, Ti, Cr, V and W in the clay component. In the fine lag it is correlated with the other alkaline earth elements Mg, Ca and Sr; the non-magnetic component shows additional correlations with Fe, As, Co, Mn, Ni and Pb. At Beasley Creek, Ba has been shown to occur as barite in the lag and is also concentrated in the cellular ironstone (gossan), but not in the calcareous component. At Mt. Percy (Butt, 1991), Ba also appears to occur in the weathered zone as barite and is not preferentially enriched in the carbonates in comparison to the ferruginous component. At Lights of Israel, its site is not clear, though it is probably located more with Fe oxides than with carbonates.

7.4 Target Elements (Au and Ag)

Gold. Gold gives the best indication of the mineralisation, with significant anomalies (400-700 ppb) in a regional background of 5-7 ppb and a contrast of 33-120. Of the soil fractions, the <4 μm fraction shows the strongest Au anomaly (750 ppb), with lesser but similar anomalies (400 ppb) from the <75 μm fraction and the complete soil (Figure 15B). Gold is strongly correlated with Ca and moderately correlated with Mg, S and As in the <4 μm soil fraction, suggesting an association with soil carbonates. The least effective fraction is the >600 μm, with a 200 ppb anomaly, which is displaced to the east of the mineralisation by 75 m. This association of Au is markedly different from the findings at Beasley Creek, where Au is associated with Fe oxides and not with carbonates.

Although the coarse lag and the non-magnetic component of the fine lag both show similar peak sizes, their Au data are characteristically spiky (Figure 15A). The fine lag accurately locates the mineralisation, with an anomaly of 200 ppb.

The soil Au anomalies (Figure 15B) were confirmed by later ditchwitch sampling to 1 m (Figure 16A) where a peak of over 1200 ppb was recorded. A small Au anomaly of over 300 ppb occurs to the west of the mineralisation but this particular sample is very Ca rich (Figure 13B). The Au/Ca relationship shows a background relationship approximating to 1% CaO to 20 ppb Au (Figure 16B). Recalculating the Au as a residual, compensating for this background relationship (Figure 16A), removes this false Au anomaly and improves the data slightly. It is possible that Ca/Au relationships could be used to improve Au data interpretation in areas of soil carbonate.

Extractable Au. It has been shown (Gray *et al.*, 1990) that some gold, associated with carbonates, is very easily extracted, using an iodide reagent. The distribution of iodide-extractable Au is illustrated in Figure 17A and B and the data are given in Appendix 19; the easily extractable Au represents about a third of the total Au. The very close correlation (r^2 = 0.95) between total and extractable Au indicates that little would be gained from calculating residuals. Both the total Au (Appendix 3) and the extractable Au (Figure 17C) follow a similar trend to that of Ca. There is a very slight decrease in correlation between the evaporitic components Ca, Mg and Na on the one hand, on passing from extractable Au to the non-extractable Au on the other, implying that the extractable Au may be co-located with pedogenic carbonate. This is very similar to results from soils from Mt. Hope (Gray *et al.*, 1990), for which it was also observed that up to 30% of the Au could be extracted by iodide from carbonate-rich soils. Other sites from the Yilgarn Block have confirmed that the high solubility of Au from carbonate-rich soils appears to be ubiquitous. This does not necessarily

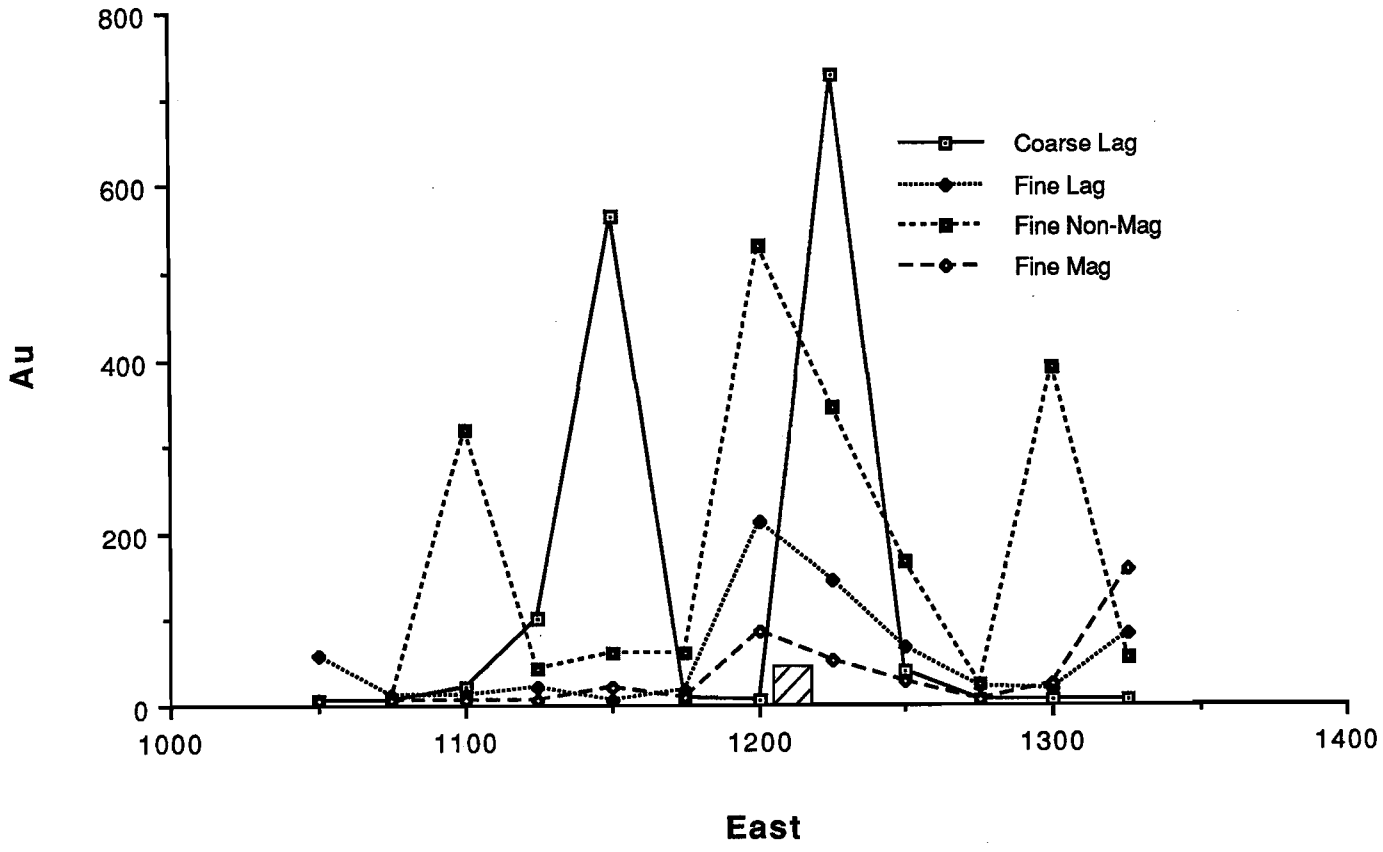

Figure 15A. Gold in lag and its components of traverse 1200 mN.

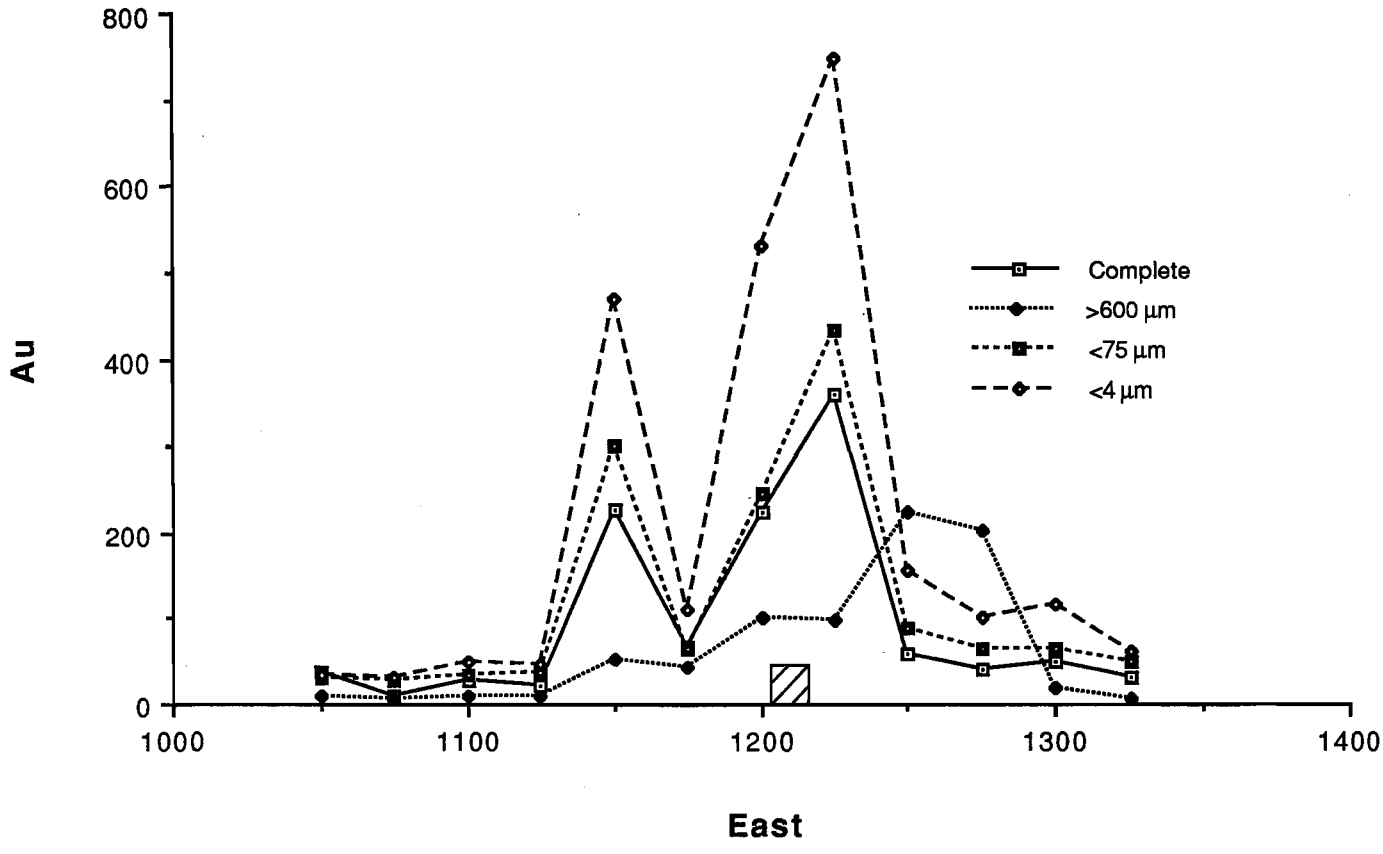

Figure 15B. Gold in soil and its fractions of traverse 1200 mN.

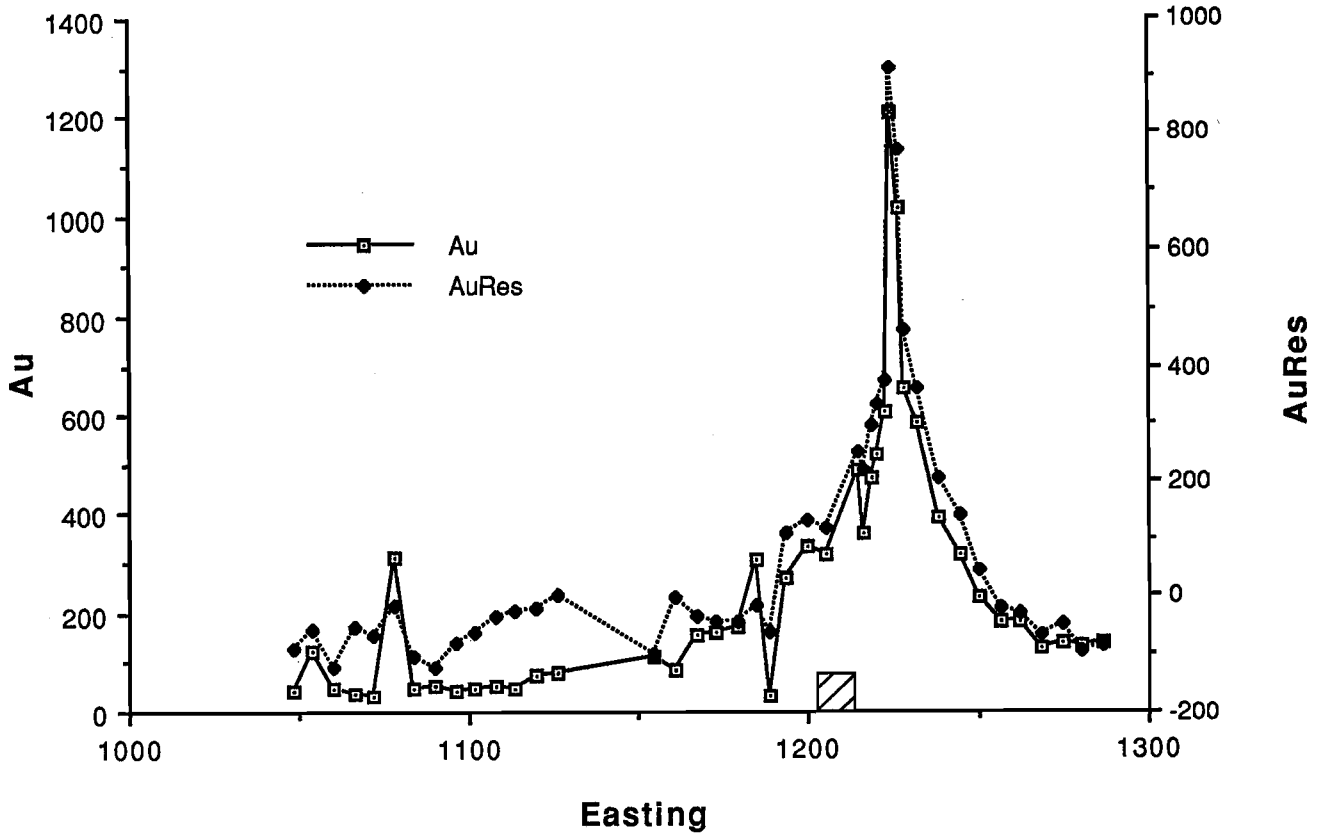

Figure 16A. Gold and Ca-related Au residual in ditchwitch traverse 1200 mN.

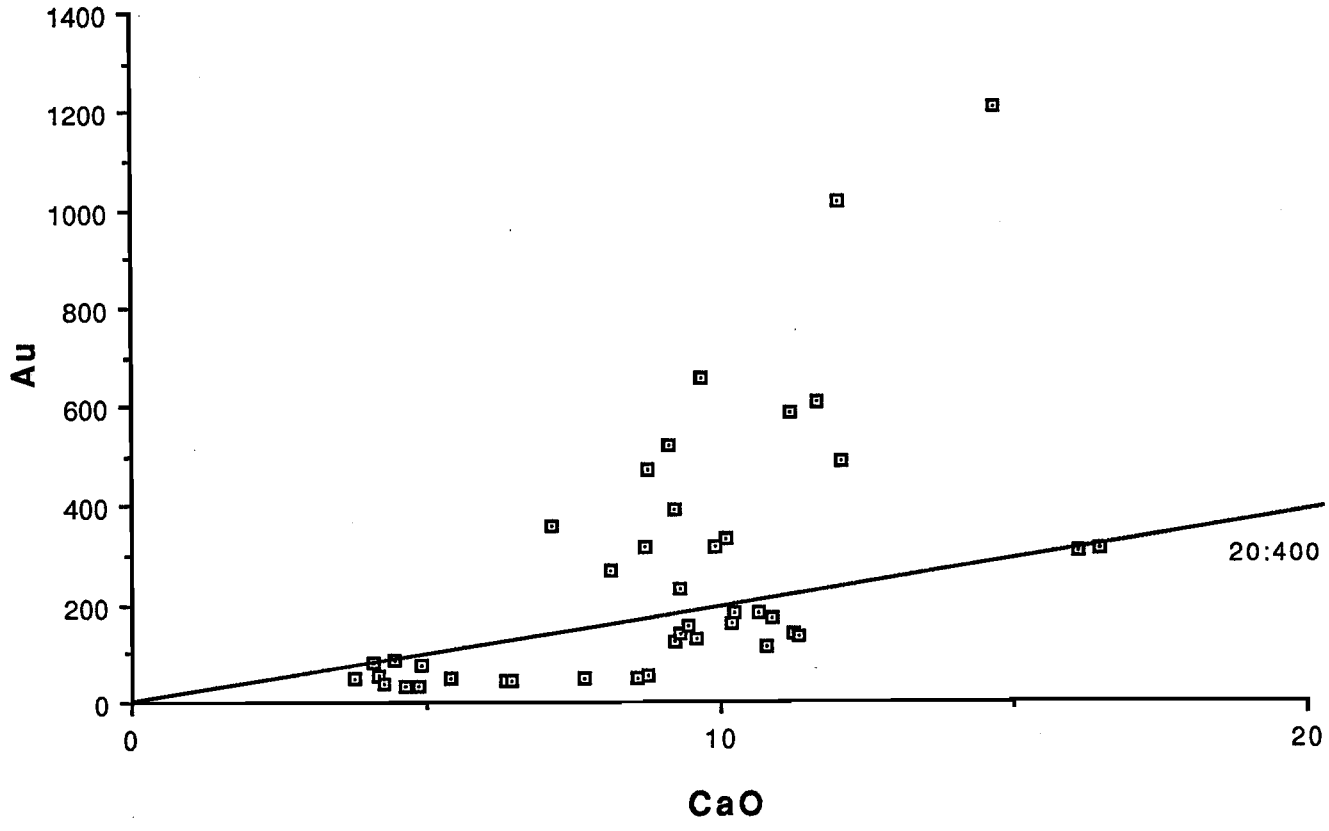

Figure 16B. Au and Ca relationship, showing background and anomalous populations from ditchwitch traverse 1200 mN.

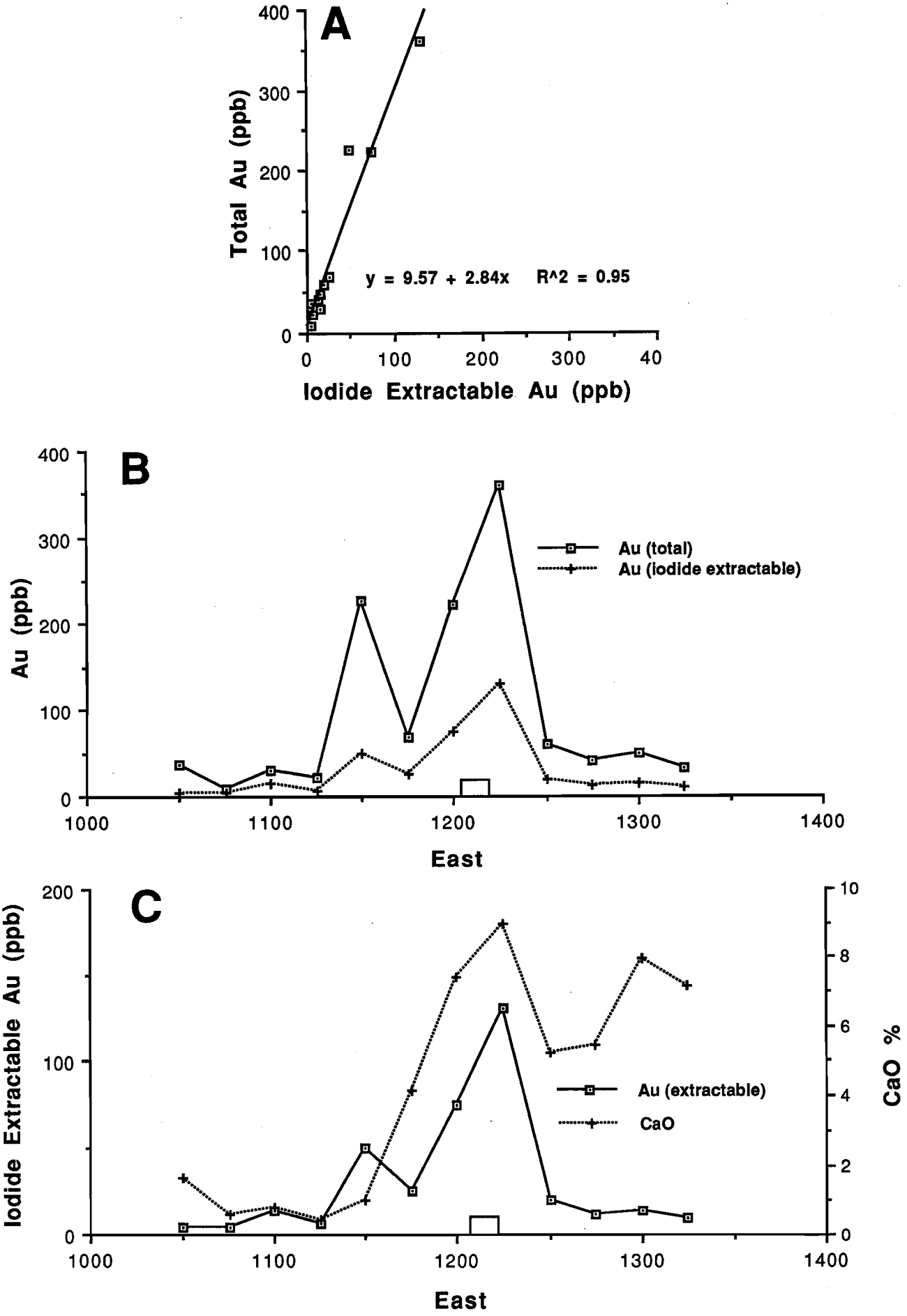

Figure 17. Relationships between total Au, iodide-extractable Au and Ca in soil from traverse 1200 mN.

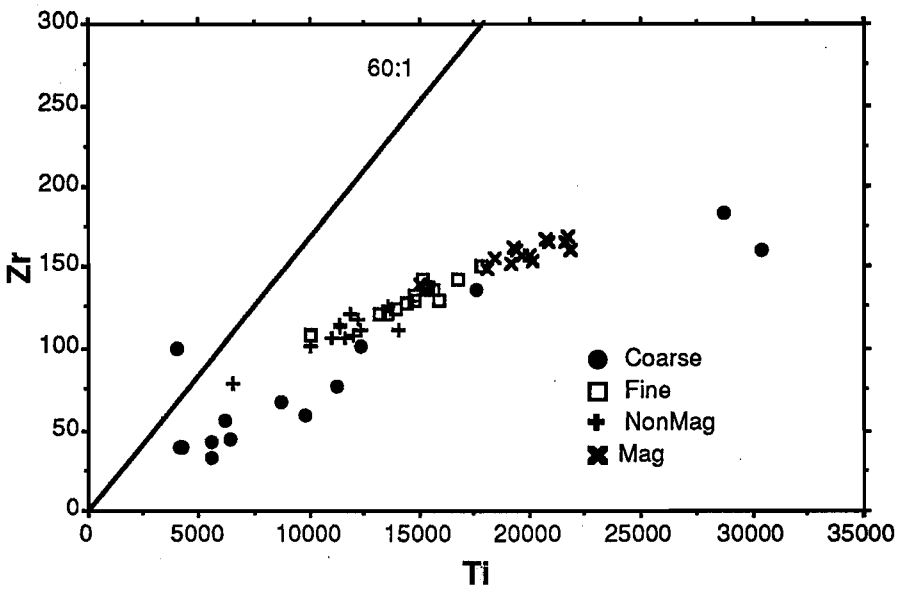

Figure 18A. Titanium and Zr relationships in lag and its components.

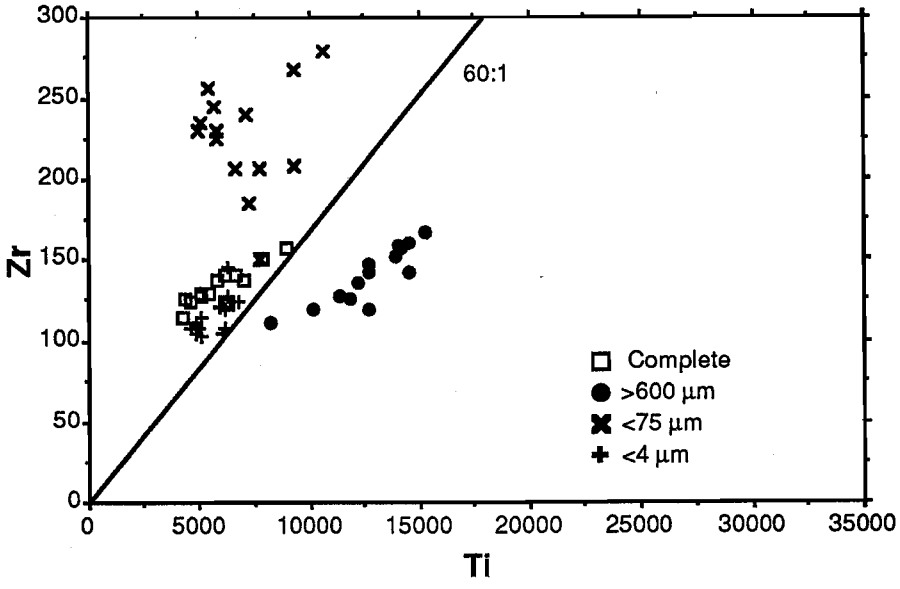

Figure 18B. Titanium and Zr relationships in soil and its fractions.

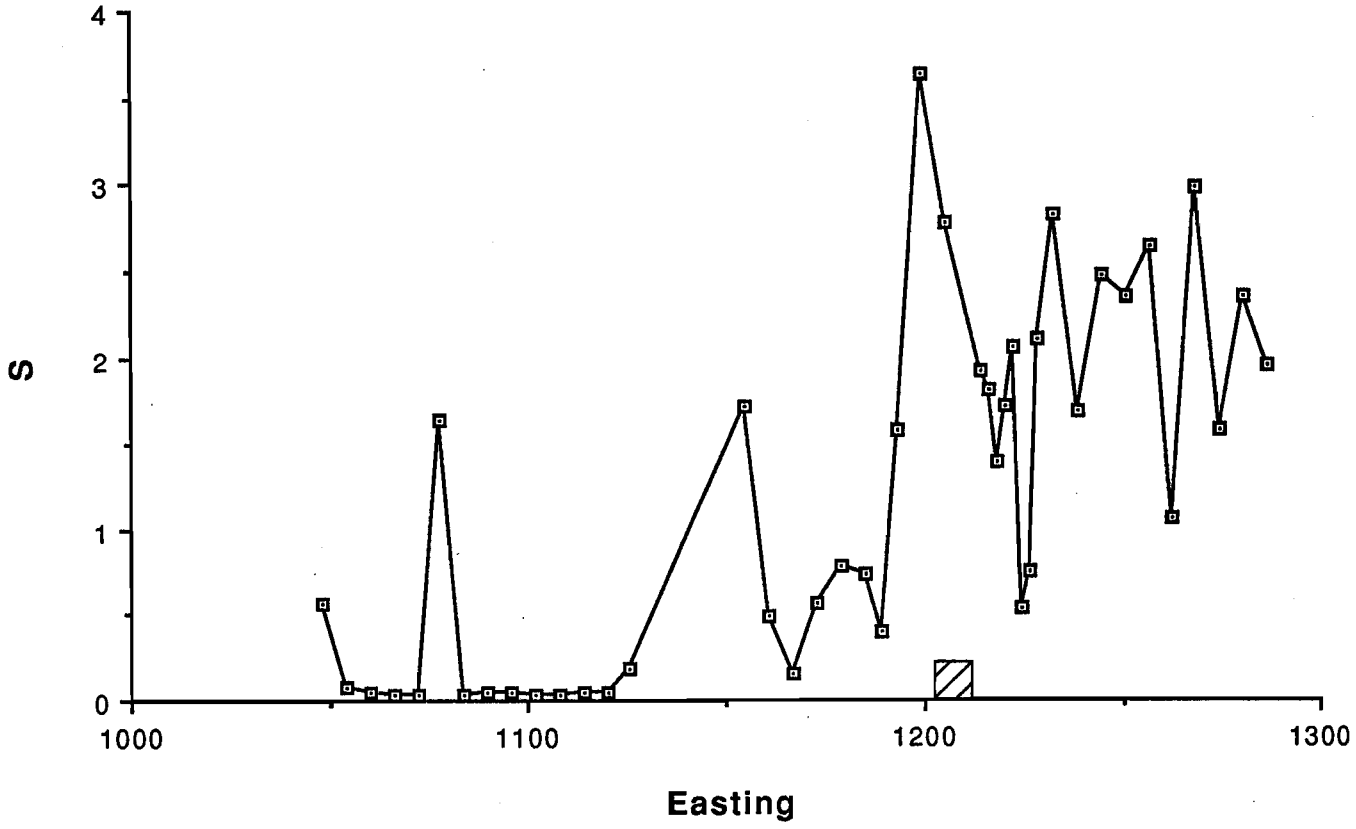

Figure 19. Sulphur content of ditchwitch traverse 1200 mN.

imply that the easily extractable Au is chemically attached to the carbonate, rather that it has been precipitated in a similar evaporitic environment.

Silver. Silver was only measured on the soil, using the very sensitive ICP/MS technique. Although the regional background in Ag (0.2 ppm) is slightly lower than that encountered near the mineralisation (0.2-0.6), the variance is sufficiently high to obscure any anomaly. Silver is highly mobile in the weathering environment.

7.5 Chalcophile Pathfinder Elements (As, Sb, Bi, Cu, Pb, Zn and Cd)

Primary mineralisation at Lights of Israel is sulphide-poor and has only low abundances of chalcophile elements. There is only a very weak anomaly in As and broad but weaker anomalies in Sb, Cu and Cd; no anomaly is detectable in Bi, Pb and Zn. However, the limited length of the geochemical traverse has led to equivocal results.

Arsenic. The As abundance in the lag (20 ppm) is nearly three times that of the fine soil fractions (5-10 ppm), which demonstrates the strong affinity of Fe oxides for As. Although the fine lag, its non-magnetic component and the >600 μm soil fraction show a weak As anomaly associated with mineralisation, the whole area sampled has a local background of about twice that of the regional background. It is suspected that the size of the As anomaly in the lag exceeds that of the sampling. There is no recognisable As anomaly in the soil except perhaps for the >600 μm fraction.

The As anomaly at Lights of Israel is much lesser (30 ppm) than that at Beasley Creek (200 ppm). At Beasley Creek, As is also preferentially enriched in the ferruginous materials, where it occurs in the non-magnetic component of the lag that has been shown to contain fragments of gossan. Gossanous material is far less abundant at Lights of Israel.

Antimony. The local Sb background for the lag is slightly higher than the regional background (by 1.2-1.7). There is also a broad but weak Sb peak over and west of the mineralisation in the ferruginous materials of both media. The Sb anomaly, if it is such, appears to be largely associated with the non-magnetic component (1.7 ppm), though the magnetic component has the highest Sb abundance (2.7 ppm). There are significant correlations with Ti, V and Zr. The precision of INAA analysis is essential to detect such a very weak response.

Bismuth. Bismuth was determined on the soil but not on the lag. Most of the data (0.2-0.3 ppm) are above the detection limit (0.1 ppm) but there is no recognisable Bi anomaly associated with the mineralisation. In the complete soil and in the >600 μm fraction, Bi is strongly correlated with In and with Pb in the <4 μm fraction. Coincident Bi peaks occur in the <75 μm and the <4 μm soil fractions, which may be related to minor Bi mineralisation from a small quartz vein at 1150 mE. No recognisable Bi anomaly was detected at Beasley Creek.

Copper. The Cu background is related, in part, to the mafic lithology. The regional Cu background is slightly lower than the Cu abundances in the traverse, particularly for the coarse lag and the non-magnetic component of the fine lag, the coarse fraction of the soil and its extremely fine fraction (200 ppm). All the geochemical media, except for the coarse lag, show a slight increase in Cu abundance to the east. This is most marked in the very fine soil fraction. It appears that there may be a very weak but broad Cu anomaly of 1.2-1.7 of regional background. A much more distinct Cu anomaly (200 m wide) was found at Beasley Creek, concentrated in the coarse, ferruginous materials and particularly in their non-magnetic components, where it is, in part, associated with gossanous fragments.

Lead. Although there is a gradual increase in the Pb abundance (20-40 ppm) from west to east in the fine lag, its components and in the >600 μm soil fraction, there does not appear to be a significant Pb anomaly in any of the surficial media investigated, unless it is very broad. Lead shows correlations with Ce, Mn and La in the ferruginous materials and does not appear to have a chalcophile association here.

Zinc. The coarse lag is much richer in Zn (300 ppm) than the fine lag (100 ppm). There is no Zn anomaly marking the mineralisation in any of the media investigated, though there is a very slight increase in Zn abundance from west to east. In the soil, the ferruginous and the clay fractions are the most Zn rich. Zinc tends to correlate with Co in the soils and some lag components.

Cadmium. Cadmium was determined on the soil and its fractions, but not on the lag. Although most of the data (0.1-0.3 ppm) lie above the ICP/MS detection limit of 0.05 ppm, no easily recognisable Cd anomaly can be seen in the soil traverse data. However, the regional background Cd data have a range of about half that of the profile data, suggesting that there is a weak (x2) but broad Cd anomaly. Thus, there appears to be a broad but very subtle Cd anomaly which exceeds the size of the traverse. There are moderate correlations between Cd and P, La and Zn in the complete soil, >600 μm and <75 μm fractions respectively. A distinct Cd anomaly (0.6 ppm) was detected at Beasley Creek, particularly in the ferruginous, coarse soil fraction, to a lesser extent in the <4 μm fraction and was presumed to also occur in the lag.

7.6 Alkalis (Na, K and Rb)

Sodium. Only the soils were analysed for Na and K. There is a marked Na peak (0.8% in a background of 0.3%) in the complete soil over the deposit. One interpretation is that it is probably related to the halite crystals (Figure 6E), found in the soil profile of a small stope near line 1200 mN. An alternative is that it is related to a paragonite (mica) content. The presence of halite implies strong surface evaporation in these locally carbonate-rich soils. Data for the soil fractions are unreliable, for halite would be lost during wet sieving. The relatively high overall Na content (0.4%) of the <75 μm fraction could represent minor paragonite or wind-blown plagioclase.

Potassium. The ferruginous >600 μm fraction is the least K rich (0.1%) and K is most abundant in the <4 μm fraction (1.0-1.5%), where there is a progressive increase in K abundance from west to east, reflecting changes in the content of fine-grained mica (sericite; Section 7). Elements strongly correlated with K in the <4 μm fraction are Rb, Mg, P, rare earth elements (Ce, La, Y), Cu and Zn. Rubidium and Mg are probably co-located with K in the mica.

Rubidium. The most Rb-rich materials (>40 ppm) are the fine soil fractions, in which there is a very strong correlation with K, REEs, Nb and Zn, indicating that the site of Rb is probably in very fine-grained micas. There is a progressive increase in the Rb abundance from west to east. The Rb abundances in the ferruginous materials of both media is at or below the detection limit of 5 ppm, so the data represent analytical noise.

7.7 Stable Indicator Elements (Ti, Zr and Cr)

Titanium. Titanium is slightly concentrated in the >600 μm fraction (2%) relative to the other fractions (1%), where it probably occurs as anatase, occluded within iron oxides. It shows no preferential concentration relative to the mineralisation. There is a wider variety of Ti concentrations found within the lag components, the magnetic component being the most Ti-rich (3.5%) and the non-magnetic component the least (2%), confirming association with Fe oxides.

Throughout the media there are strong to moderate correlations of Ti with Fe, Cr, Ga, Sb (soil), Nb (lag), V and Zr.

Zirconium. Zirconium, where it occurs as zircon, is generally very stable and concentrates as a resistate mineral but, where it occurs in other minerals, it is less stable and weathers with them. Even zircon may be corroded and its stability may be significantly reduced if damaged by radiation. Dissolved zirconium may be fixed by clays or hydrolysed to colloidal particles (see Erlank *et al.*, 1978). The coarse lag and the non-magnetic component of the fine lag are the least Zr rich; the <75 μm fraction of the soil contains the most Zr and the <4 μm fraction the least. Zirconium is consistently correlated with Ti and V in almost all media and is commonly correlated with Fe and Ga in the ferruginous materials. Zirconium probably occurs as zircon in the silty <75 μm fraction.

Ti/Zr Ratio. The Ti/Zr relationship (Figure 18A) in the lag (apart from one sample of coarse lag) indicates a very consistent basaltic composition (>60:1; Hallberg, 1984). The lag appears to have been derived from ferruginised saprolite, so its Ti/Zr ratio is likely to have remained relatively undisturbed by Ti loss (Butt *et al.*, 1991). The ferruginous >600 μm fraction of the soil is similar to the fine lag (Figure 18B) but the >75 μm soil fraction is markedly more Zr-rich, apparently reflecting an increase in residual zircon or in extraneous zircons imported by aeolian action.

Chromium. The fine lag and its components are significantly richer in Cr than the coarse lag, which shows noisy data. The >600 μm soil fraction is significantly richer in Cr than the fine soil components. Chromium is strongly correlated with Ti in the soil, its fractions, in the non-magnetic lag component and, to a lesser extent, with Fe, Ga and V. It is assumed that much of the Cr is contained in Fe oxides (similar to Beasley Creek, where the Cr abundance is also much lower in the coarse lag). There is no ore-associated Cr anomaly and the relatively flat response reflects a consistent (mafic) lithology, which is less chromiferous than the mafic-ultramafic bedrocks at Beasley Creek.

7.8 Metalloids (P and S)

Phosphorus and S were determined only on the soil. The results suggest no relationship to the mineralisation, though, in the <4 μm fraction, there is a progressive increase in P to the east of the drainage (0.04-0.12%). There is strong correlation in the clay fraction with Mg, K, Ce, Cu, Y and Zn and moderate correlation with S, Mn, Ni, Pb and Rb; there is little correlation of P with other elements in the other soil fractions.

Sulphur. The whole area is markedly anomalous (0.4-0.8%) in S, compared to the regional background (0.02%). There is a peak in the S abundance in the complete soil and in the <4 μm fraction above mineralisation but there is also an area of elevated S to the extreme west. The coarser fractions, particularly the >600 μm fraction are uniformly low in S (0.02%).

The variations reflect inconsistencies in sampling. Greater variations could have occurred if samples had been collected deeper and had sporadically collected the layer of coarse gypsum at the base of the soil carbonate horizon (Section 4.3). This is illustrated by the ditchwitch traverse (Figure 19). This emphasises the background area to the west of the drainage (0.04% S) and the anomalous nature of the area overlying the mineralisation (2% S). Anomalous S abundances (0.1 in a background of 0.02%), as gypsum ($CaSO_4.2H_2O$) and minor barite ($BaSO_4$), were noted in the soil and in the saprolite (1.6% S) above the Beasley Creek orebody (Robertson, 1990; 1991). This S anomaly was also most marked in the <4 μm soil fraction.

Sulphur Isotopic Ratio. The origin of the S, *i.e.* whether it is derived from oxidised sulphides or is meteoric, was investigated with a sulphur isotope study. Near the coast, isotopically heavy S is precipitated from an aerosol of particulate gypsum, derived from the sea and carried inland by the dominant south-westerly winds. Further inland there is a proportionally greater influence of rainfall-precipitated isotopically lighter, though also ocean-derived, gaseous, organic S compounds. Thus, on a regional scale in Western Australia, the $\delta^{34}S$ values of surficial gypsum form a gradient over distances of 500-1000 km, with highest values of 21 near the coastline, decreasing to 14 further inland (Chivas *et al.*, 1991). Significant negative deviations from this meteoric pattern would indicate a bedrock source of some of the S. The meteoric $\delta^{34}S$ background at Davyhurst would be expected to be 18.3‰.

The gypsum horizon, overlying the southern extension of the mineralisation, was exposed in the costean (Figure 7). The isotopic composition of the sulphur in this gypsum was examined. Five samples (LOI-101 to LOI-105) of the gypsum horizon were collected along this trench and two from a small stope near line 1200 mN (LOI-001 to LOI-002). A soil sample from above (LOI-06) and one from below the gypsum horizon (LOI-107) were also collected. All were found to have small quantities of S. The S isotopic ratios (A. Andrew, pers comm.,1988; Chivas *et al.*, 1991) are given in Table 5; these ratios average 17.1‰ and are slightly (1.2‰ or 2σ) lower than the interpolated local meteoric background. Although this S is dominated by seawater sulphur, the isotopic signature may contain a component of bedrock S.

TABLE 5
Sulphur Isotopic Ratios
Soil Gypsum - Lights of Israel Mine

Sample	$\delta^{34}S$‰
LOI-001	16.2
LOI-002	17.8
LOI-101	17.7
LOI-102	16.8
LOI-103	17.8
LOI-104	17.3
LOI-105	16.9
LOI-106	16.2
LOI-107	17.3
Mean	17.1
Std Dev	0.63

7.9 Transition Elements (Mn, Co and Ni)

Manganese. The Mn plots for all surficial materials show a marked increase in abundance, from 1200 to 4000 ppm, to the east in all ferruginous materials. The Mn abundance in the fine soil fractions is relatively constant at 1000-1800 ppm. Manganese can be strongly concentrated in lateritic regoliths and Mn minerals generally have a variety of trace elements either adsorbed onto their surfaces or co-precipitated with them. The ferruginous materials of both media show Mn correlations with Ce, La and Pb and the local Mn background is greater than the regional background; the clay-rich materials show significant correlations of Mn with Co and Zn. Manganese does not appear to be related directly to the mineralisation but perhaps to its halo.

There is a very strong Mn association with the ore host at Beasley Creek (Robertson and Gall, 1988; Robertson, 1989; Robertson, 1990; Robertson, 1991).

Cobalt. The coarse lag has a very erratic Co content (30-300 ppm); the fine lag and its components and the soil and its fractions are relatively consistent (25-45 ppm). Both regional and local background abundances are similar. There is no detectable anomaly in any of the Co data. Cobalt is mobile during weathering, but is commonly co-precipitated with Mn oxides; it is moderately to strongly correlated with Ni, Mn and Zn in several media. No Co anomaly and very similar Co abundances were encountered at Beasley Creek, where less variance was found in the Co soil data over Permian glacial tillites than over weathered and partly stripped Archaean rocks. The Co variance at Lights of Israel is similar to that of the Archaean of Beasley Creek.

Nickel. The highest Ni concentrations (130-200 ppm) occur in the <4 μm fraction of the soil and less so in the >600 μm fraction. Nickel is abundant in the coarse lag (200 ppm) and least abundant in the non-magnetic component of the fine lag (110 ppm). There is a slight increase in the Ni abundance towards the east in all sample media, except for the coarse lag, where there is much, probably random, variation. The highest Ni concentrations occur in the red-brown clays of the lag at Beasley Creek (Robertson, 1989), indicating significant Ni mobility in the ferruginous rocks at the top of the lateritic profile, where Ni is known to be mobile under acidic, oxidising conditions. Nickel is correlated with Co, Cu and Zn in the ferruginous materials but there is no relationship between Ni and the mineralisation at Lights of Israel. The Ni and Cr abundances in all the media are typical of and confirm underlying mafic rocks.

7.10 Rare Earth Elements (Ce, La and Y)

Cerium. The abundance of Ce in the fine lag and in the >600 μm soil fraction increases towards the eastern part of the section. This increase is weaker in the fine soil fractions and is absent in the coarse lag. Cerium is strongly correlated with La in all media but with Y only in the less-ferruginous media. Cerium is also moderately correlated with Cu, Pb, Rb and Mn, suggesting it is sited in various resistate minerals and/or manganese minerals.

Lanthanum. The coarse (>600 μm) soil and all components of the fine lag are richer in La than in the finer soil fractions. The La abundance, similar to that of Ce, increases to the east in the ferruginous media. Lanthanum is strongly correlated with Ce and Mn; to a lesser extent, with Pb, Cu, Y and Zn. Association of La with Fe and Mn oxides seems probable.

Yttrium. Yttrium is considered with the rare earth elements because of chemical similarity. There is a slight decrease in the abundance of Y over the mineralisation in the fine-grained ferruginous materials. In contrast, the soil and its fine fractions show a progressive increase in Y content from west to east. Yttrium correlates moderately to strongly with La, Cu and Ce in all soil fractions. This increase in Ce, La and Y on the east part of the traverse may reflect a greater abundance of felsic dykes.

7.11 Granitoid Associated Elements (Mo, Nb, Sn, Be and W)

The abundances of these elements, particularly Mo and Be, were at or below detection limits in most samples, apart from some erratic single point peaks. It is possible that there is some weak concentration of Nb in the fine soil fractions, similar to Beasley Creek but this may refelect a matrix effect.

Tin. Tin was only determined in the soils, by ICP/MS analysis (detection limit 0.5 ppm). There appears to be a single point Sn anomaly (3 ppm) over the mineralisation in the <4 μm fraction and possibly a weak anomaly (2.3 ppm) in the >600 μm fraction. The <75 μm fraction and

the complete soil show background abundances of 1.5 ppm. Tin is correlated with Ag and Cr in the <75 μm fraction and with Ca, Sr and Au in the <4 μm fraction. It is possible that the Sn may be related to granite-related quartz-tourmaline veinlets rather than to Au mineralisation.

Tungsten. The regional W background is significantly less than the local W background but much of the W data lie close to or below the detection limit of 5 ppm. The lag is slightly richer (8 ppm) in W than the soil (2 ppm). A single point peak (28 ppm) in the coarse lag lies close to the subcrop of a small quartz vein exposed by ditchwich sampling. The elevated W content of the ferruginous materials suggests that W may have been coprecipitated with Fe oxyhydroxides as some form of tungstic oxide (see Krauskopf, 1978).

7.12 Microprobe Analysis of Tourmalines

Compositions of tourmalines from a veinlet at 44 m depth (1020 mN, 1060 mE and 414 R.L) were compared with those of tourmalines which occur in almost all soil fractions, to determine if they constituted a single population. If they were geochemically identical it would strongly support a residual origin for much of the soil.

The fresh sample (LOI-113) is a highly inhomogeneous material. The wallrock consists of matted, acicular, coarse-grained actinolitic amphibole and plagioclase and the vein material is of acicular tourmaline (schorl) cut by later quartz. The tourmaline (Figure 6A) contains patches of epidote, chlorite and highly sausseritised plagioclase, probably representing included fragments of highly altered wallrock.

Step scanning of a single grain from soil sample LIC-52 showed that there is little significant compositional variation due to zoning (Fig 20; Appendix 20). This was confirmed by subsequent analysis of the cores and rims of numerous grains from soil samples LIC-53 and LIC-58. The results are tabulated in Appendix 15. The Fe Number (Fe#), as defined by Pirajno and Smithies (1992) as FeO/(FeO+MgO) has also been calculated. Examination of quantile-quantile plots of each major element indicated a single population. Chromium, which is not a part of the tourmaline molecule, showed two populations and probably reflects submicron-sized inclusions. Sodium, which is part of the tourmaline lattice, also appeared to show a second but minor population at low Na contents ($<1.5\%$). This element has a low atomic number, and is not very stable in the electron beam, so it is possible that the analysis may be less reliable than that of the other elements. Bivariate examination of the data supported the conclusion of a single tourmaline population, with the exception of Na and Cr. The data from soil sample LIC-58 are more tightly grouped than that for LIC-53. The greater tourmaline abundance and its lesser geochemical variance in the former sample suggests it is closer to the source of the tourmaline.

Data from 53 tourmalines from the fresh vein (LOI-113) are very consistent (Appendix 15). A comparison between the vein and soil tourmalines shows that the former are more tightly grouped but otherwise indistinguishable from the latter (Figure 21). It is concluded that the tourmaline veinlets, as exemplified by specimen LOI-113, are a very likely source of the soil tourmaline and that the soil is largely residual. It is also concluded, from the work of Pirajno and Smithies (1992), that these tourmalines have an intermediate to distal relationship (Figure 22) to their source pluton and form a single population.

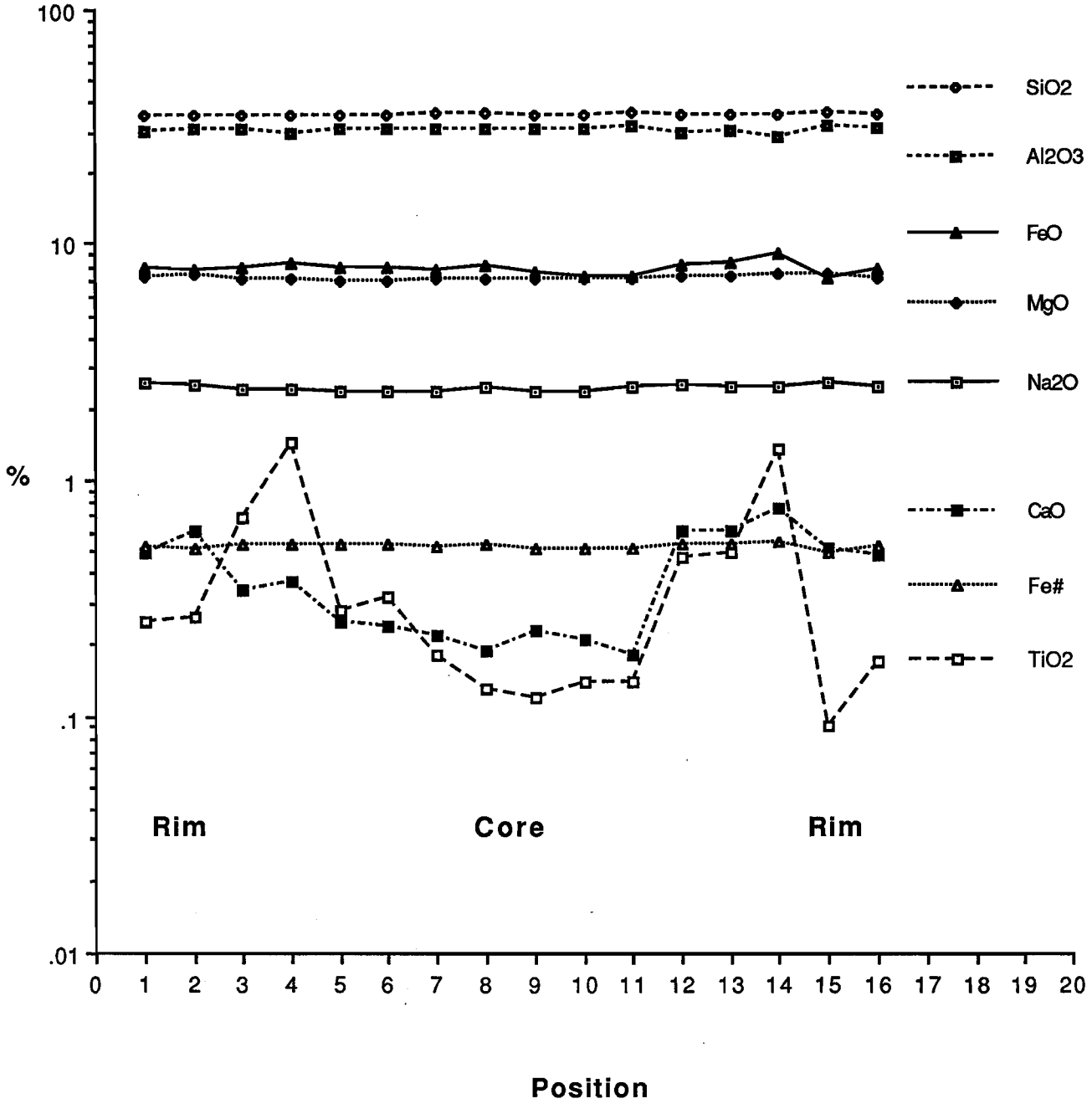

Figure 20. Microprobe traverse from rim to rim across the short dimension of a tourmaline grain to demonstrate a lack of zoning.

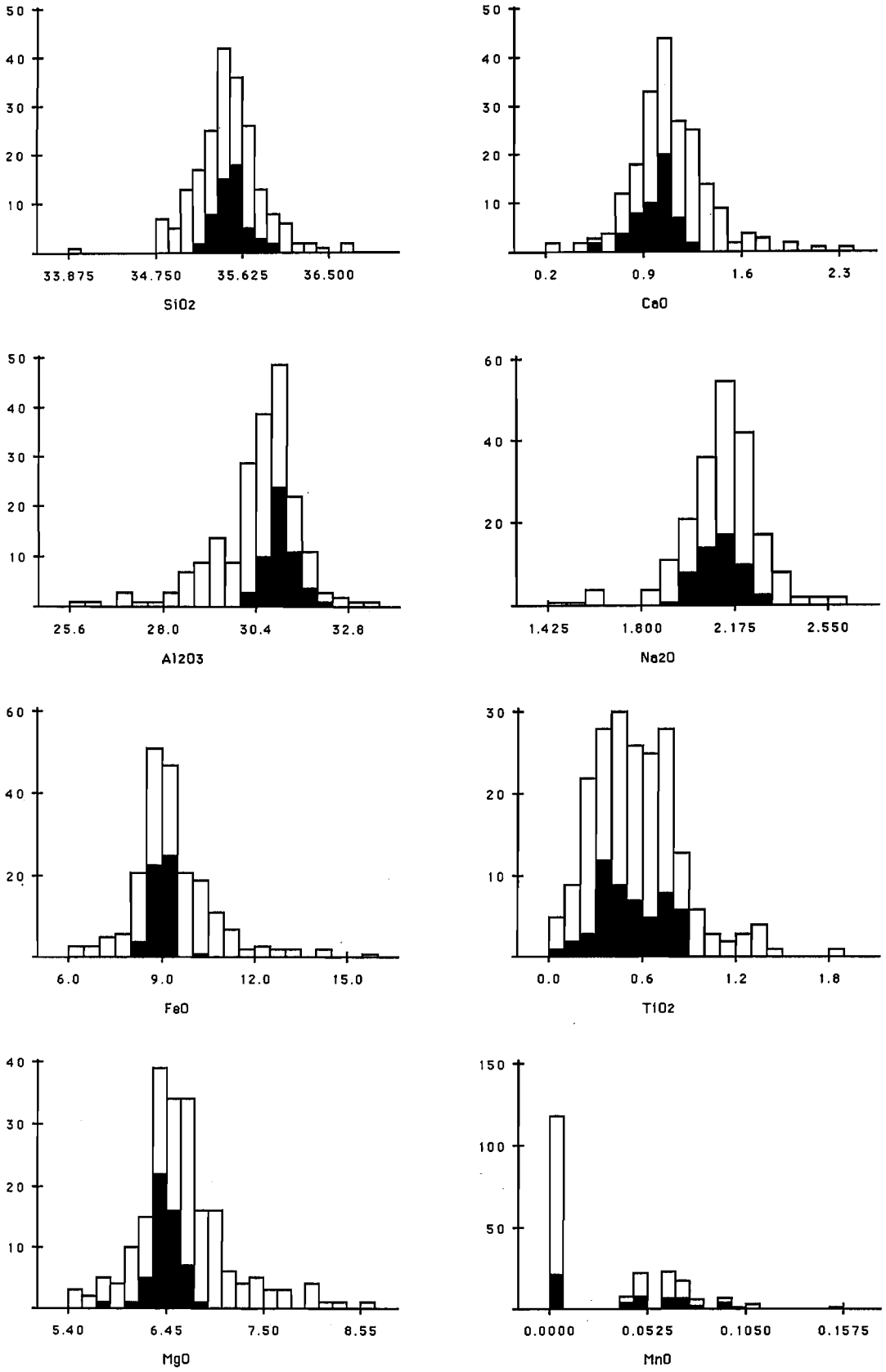

Figure 21. Distributions of Si, Al, Fe, Mg, Ca, Na, Ti and Mn of soil tourmanlines (white) and fresh tourmalines (black) showing that they are indistinguishable.

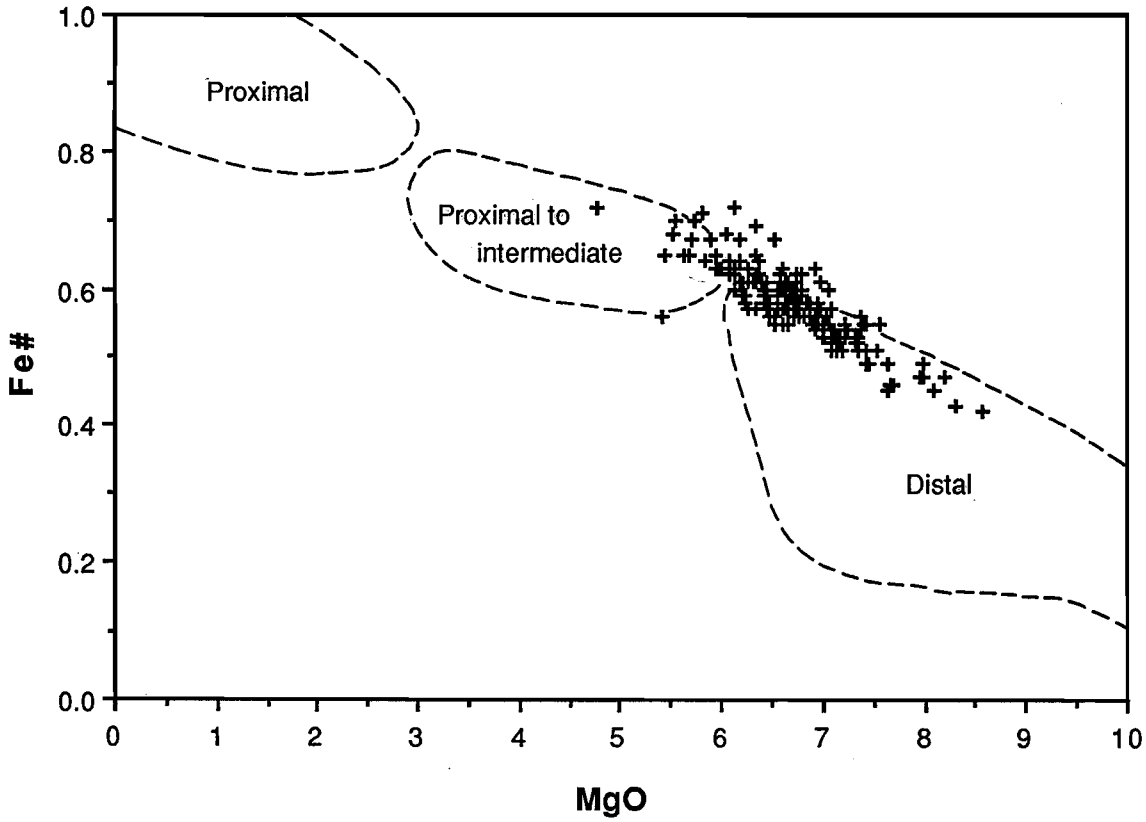

Figure 22. Plot of Fe# against MgO (after Pirajno and Smithies, 1991) suggesting an intermediate to distal relationship of the Lights of Israel tourmalines to their source pluton.

8.0 SUMMARY AND CONCLUSIONS

8.1 Geology and Composition of Soil and Lag

The mine site at Lights of Israel is mantled by a thin, largely residual soil, overlying a lateritic profile, truncated to the saprolite. The soil is alkaline in its upper part, being rich in carbonates. This layer is underlain by a discontinuous gypsiferous horizon which, in turn, is underlain by carbonate-free brown clay soil and by saprolite.

The soil consists of a mixture of three contrasting fractions. The coarse fraction (>600 μm) is comprised of dense, goethitic as well as slightly less-dense, ferruginous, clay pebbles and granules, with a few quartz grains. The intermediate fraction (75-600 μm) consists largely of bright, clear and angular quartz sand and silt, with minor grains of feldspar, and small ferruginous granules. The fine fraction (<75 μm) consists of quartz grains and smaller kaolinite and iron oxide particles (<1 μm).

Each fraction apprears to be locally derived, although there is a small, wind-blown component which increases in abundance as the material becomes finer. This aeolian component is much smaller than that encountered at Beasley Creek (Robertson, 1990). The fine fraction was also probably largely derived by mechanical breakdown of clay pisoliths and granules. Later deflation of the upper soil layers, by wind and water, has left a discontinuous covering of lag.

The ferruginous granules of the coarse soil fraction are petrographically indistinguishable from the lag, for which they provided the source. Petrography of the interiors of goethitic granules reveal relict sericite near the mineralisation and goethite pseudomorphs after saprolitic kaolinite, as well as vermicular, pedogenic accordion structures, all set in a variety of secondary goethite (massive, spongy, vesicular, colloform). Minor gossan fabrics, from close to the mineralisation, suggest derivation from fine-grained pyrite and the lag had suffered little subsequent mechanical dispersion.

8.2 Mineralogy

The mineralogy of the soil is more complex than that of Beasley Creek. *Quartz* occurs as fragments of white vein quartz but dominantly as clear, glassy, sharp crystals, some with drusy terminations. *Kaolinite* and *smectite* form separate, clay-sized particles but also form a component of coherent clay pisoliths and granules. The iron oxides, ***hematite, maghemite and goethite***, which form loose, clay-sized particles, also occur as major components of black, dense granules and form minor components of clay-rich granules. *Sericite* occurs particularly in the clay fraction, close to the mineralisation and may constitute a phyllic halo. Fragments of fresh, sharp *tourmaline* crystals form a minor but important soil component, whose consistent composition and similarity to the tourmaline of nearby quartz-tourmaline veinlets confirms that much of the soil at Lights of Israel is residual. *Calcite* occurs as very fine pedogenic particles. There is also minor anatase and K-feldspar.

North of the Menzies Line, particle size fractionation has shown that the >600 μm fraction has considerable potential as a geochemical sampling medium, because of its high Fe oxide content. However, at Lights of Israel, south of the Menzies Line, the carbonate-rich parts of the soil, be they fine or coarse, are by far the best for Au geochemistry.

Quartz and feldspar are concentrated in the <75 μm fraction and even more so in the discarded 75-710 μm fraction, which contain the bulk of this diluting material. Kaolinite and smectite are concentrated in the <75 μm fraction and particularly in the <4 μm fraction. Calcite occurs

mainly in the <75 μm fraction; it appears to have been largely removed from the <4 μm fraction by acidification of the clay suspension.

Plots of the abundances of sericite and calcite show maxima, located over the mineralisation in this near-surface soil. Calcium analysis of alternate samples, collected from the top metre, suggest that this calcite maximum is an artifact of sampling depth. The sericite anomaly is no doubt real.

8.3 Geochemistry

The soil and lag traverses at Lights of Israel were short, due to limitations imposed by the availability of lag and by the small size of the mine leases and do not extend sufficiently into geochemical background. An approximate geochemical background has been established, using two samples collected north and south of the centre of the pit. Although some pathfinder elements (As, Sb, Cu and Cd) did not give a recognisable peak in the traverse, their general abundance was significantly above that of regional background. The only distinctive anomaly is given by Au, shown by the lag and particularly by the fine soil fractions.

The major element chemistry of the media components reflects their overall mineralogy. There is a trend towards decreasing Al to the east, reflecting a decline in the abundances of kaolinite and smectite, with increasing Fe, Ca and K (Fe oxides, calcite and sericite). It seems the variation in the Ca content is related to sample depth; deeper sampling by ditchwitch gave more consistent results. Anomalies in K and Rb seem to be related to a phyllic alteration halo around the mineralisation.

The high Ti-Zr ratio (>1:60) and the Cr and Ni contents of the ferruginous materials (lag and >600 μm soil fraction), indicate a mafic origin. This is in keeping with the local basaltic host lithology. The fine soil components are all either enriched in Zr or depleted in Ti.

The whole area over the mineralisation is anomalous in S relative to regional background, due to the layer of gypsum in the soil. The isotopic composition of this S is slightly heavier (1.2 than that which would be expected if the S were derived from meteoric sources alone, thus there could be some bedrock S component.

8.4 Exploration Implications and Comparisons

i As at Beasley Creek, the soil consists of three contrasting size fractions, a coarse, granular, ferruginous fraction, a silty, quartz-rich fraction and a ferruginous, clay-rich fraction. However, the aeolian component of the silty fraction is relatively small and is largely confined to its finer parts.

ii Gold anomalies in the soil (230-750 ppb) are about 125 m wide (only slightly wider than the supergene mineralisation, 40-60 μm), show highest contrast in the fine fractions and are strongly associated with soil carbonates. This differs with the conclusions from Beasley Creek, where the greatest Au abundances (200-400 ppb) occur in the ferruginous 710-4000 μm fraction and the anomaly is very wide (800 m). Thus, Au soil sampling strategy, in areas of laterite truncation, must be controlled by a good orientation survey or at least by the relationship of the sampling area to the Menzies Line. North of the Menzies line, the ferruginous soil fraction is the most effective, south of the Menzies Line, the carbonate-rich part of the soil is the best.

iii The association of Au anomalies with carbonates is very important south of the Menzies Line. In this instance, the soil carbonates are fine grained but they may be coarse in other localities.

iv Gold anomalies in the lag (80-720 ppb) are narrower (75 m), more erratic, particularly in the coarse lag, and less well-defined. The coarse lag at Beasley Creek was similarly spikey but locally much more Au-rich (1300 ppm).

v There is no broad, chemical Au dispersion at Lights of Israel like that at Beasley Creek. The anomaly directly overlies the updip extension of the primary and secondary mineralisation.

vi Apart from the relatively distinct Au anomaly, anomalies in As, Sb, Cu and Cd, which make up the multi-element signature of Beasley Creek, are very weak and subtle at Lights of Israel. They are likely to be missed in a large-scale geochemical survey unless there is very careful control of the analytical process and geochemical background is properly established.

vii Bedrock lithology can be identified by petrographic examination of coarse lag fragments. Despite the low sulphide content of the primary mineralisation, gossan fragments were found in the lag and indicated very limited mechanical dispersion.

viii Sericite in the complete soil and the <4 μm fraction, as well as K and Rb may be related to a phyllic alteration halo around the ore.

ix An orientation study of the soil components is necessary to establish which parts contain transported materials and which parts are the best geochemical media.

x Regolith-landform mapping is essential prior to a geochemical survey. Despite the close association of gold with carbonates south of the Menzies Line, marked differences are likely in background abundances and thresholds in different erosional environments.

9.0 ACKNOWLEDGEMENTS

Sample preparation of the lag was by J.F.P. Crabb and A. Janes. In-house XRF geochemical analyses were performed by M.K.W. Hart and M. Cheeseman, and the ICP analyses by J.E. Wildman and G.D. Longman. INAA analysis was by Becquerel Laboratories and ICP/MS analysis by Analabs. Soluble Au was iodide extracted by D.J. Gray and G.D. Longman. XRD data were collected by M.K.W. Hart. Thin and polished sections were prepared by R.J. Bilz. Assistance on the SEM and microprobe was ably given by B.W. Robinson and G.J.H. Hitchen. H.M. Churchward provided geomorphological input. Drafting and artwork was by A.D. Vartesi and C.R. Steel; J. Porter checked and formatted the final document. Bardoc Gold Pty., Ltd., allowed access to their property and provided all necessary plans and geological information. All this is acknowledged with appreciation. Thanks also go to C.R.M. Butt and R.E. Smith who provided critical comment on the manuscript.

10.0 REFERENCES

Anand, R.R., Smith, R.E., Innes, J., Churchward, H.M., Perdrix, J.L., and Grunsky, E.C. 1989. Laterite types and associated ferruginous materials, Yilgarn Block, WA.; terminology, classification and atlas. CSIRO Division of Exploration Geoscience, Restricted Report 60R.

Brindley, G.W. 1980. Quantitative X-ray mineral analysis of clays. In G.W. Brindley and G. Brown (eds). Crystal structures of clay minerals and their X-ray identification. Mineralogical Society Monograph No 5. 411-438.

Box, G.E.P., and Cox, D.R. 1964. Ananalysis of transformations, Jl. R. statist. Soc., Series B, 26. 211-252.

Burton, J.D. and Culkin, F. 1978. Gallium. In K.H. Wedepohl (ed). Handbook of Geochemistry. Springer-Verlag. New York.

Butt, C.R.M. 1991. Dispersion of gold and associated elements in the lateritic regolith, Mystery Zone, Mt. Percy, Kalgoorlie, Western Australia. CSIRO Division of Exploration Geoscience, Restricted Report 156R. 226pp.

Butt, C.R.M., Gray, D.G., Lintern, M.J., Robertson, I.D.M., Taylor, G.F., and Scott, K.M. 1991. Gold and associated elements in the regolith - dispersion processes and implications for exploration. Final Report. CSIRO Division of Exploration Geoscience, Restricted Report 167, 114 pp.

Chivas, A.R., Andrew, A.S., Lyons, W.B., Bird, M.I. and Donnelly, T.H. 1991. Isotopic constraints on the origin of salts in Australian playas. 1. Sulphur. Palaeogeography, Palaeoclimatology, Palaeoecology. 84. 309-332.

Erlank, A.J., Smith, H.S., Marchant, J.W., Cardoso, M.P. and Ahrens, L.H. 1978. Zirconium. In K.H. Wedepohl (ed). Handbook of Geochemistry. Springer-Verlag. New York.

Gray, D.J. 1988. The aqueous chemistry of gold in the weathering environment. CSIRO Division of Exploration Geoscience, Restricted Report 4R, 65 pp.

Gray, D.J., Lintern, M.J. and Longman, G.D. 1990. Chemistry of gold in some western Australian soils. CSIRO Division of Exploration Geoscience, Restricted Report 126, 62 pp.

Grunsky, E. 1991. Strategies and methods for the interpretation of geochemical data. Discussion Paper applied to laterite geochemistry. CSIRO/AMIRA Project P240. CSIRO Division of Exploration Geoscience. 77p.

Hallberg, J.A. 1984. A geochemical aid to igneous rock identification in deeply weathered terrain. Journal of Geochemical Exploration, 20. 1-8.

Hart, M.K.W. 1989. Analysis for total iron, chromium, vanadium and titanium in varying matrix geological samples by XRF, using pressed powder samples. Standards in X-ray analysis. Australian X-ray Analytical Association (WA Branch) Fifth State Conference. 117-129.

Heinrich, E.W. 1978. Niobium. In K.H. Wedepohl (ed). Handbook of Geochemistry. Springer-Verlag. New York.

Hellsten, K. J., Colville, R. G., Crase, N.J. and Bottomer, L. R. 1990. Davyhurst gold deposits. In F.E. Hughes (ed). Geology of the mineral deposits of Australia and Papua New Guinea. Australasian Institute of Mining and Metallurgy Monograph No 14. 367-371.

Koritnig, S. 1978. Phosphorus. In K.H. Wedepohl (ed). Handbook of Geochemistry. Springer-Verlag. New York.

Krauskopf, K.B. 1978. Tungsten (Wolfram). In K.H. Wedepohl (ed). Handbook of Geochemistry. Springer-Verlag. New York.

Lavrenchuk, V.N. and Tenyakov, V.A. 1962. Distribution of gallium in bauxites. Geochemistry (USSR) p 862.

Avrenchuk, V.N. and Tenyakov, V.A. 1963. Gallium balance in bauxites. Dokl. Akad. Nauk SSSR 151, 1430; Chem. Abstr. 59, 15069f.

Linn, T.A. (Jr.) and Schmitt, R.A. 1978. Indium. In K.H. Wedepohl (ed). Handbook of Geochemistry. Springer-Verlag. New York.

Lintern, M.J. 1989. Study of the distribution of gold in soils at Mt. Hope, Western Australia. CSIRO Division of Exploration Geoscience, Restricted Report 24R, 36 pp.

Lintern, M.J., Churchward, H.M., and Butt, C.R.M. 1990. Multi-element soil survey of the Mount Hope area, Western Australia. CSIRO Division of Exploration Geoscience, Restricted Report 109R, 76 pp.

Lintern, M.J., and Scott, K.M. 1990. The distribution of gold and other elements in soils and vegetation at Panglo, Western Australia. CSIRO Division of Exploration Geoscience, Restricted Report 129R, 96 pp.

Norrish, K. and Chappell, B.W. 1977. X-ray fluorescence spectrometry. In J. Zussman (ed). Physical methods in determinative mineralogy. Academic Press, London. 201-272.

Pirajno, F., and Smithies, R.H. 1991. The FeO/(FeO+MgO) ratio of tourmaline: a useful indicator of spatial variations in granite-related hydrothermal mineral deposits. Journal of Geochemical Exploration. 42. 371-381.

Robertson, I.D.M. 1989. Geochemistry, petrography and mineralogy of ferruginous lag overlying the Beasley Creek Gold Mine - Laverton, WA. CSIRO Division of Exploration Geoscience, Restricted Report 27R, 180 pp.

Robertson, I.D.M. 1990. Mineralogy and geochemistry of soils overlying the Beasley Creek Gold Mine - Laverton, WA. CSIRO Division of Exploration Geoscience, Restricted Report 105R, 158 pp.

Roberton, I.D.M. 1991. Multi-element dispersion in the saprolite at the Beasley Creek Gold Mine, Laverton, Western Australia. CSIRO Division of Exploration Geoscience, Restricted Report 152R, 122 pp.

Robertson, I.D.M. and Churchward, H.M. 1989. The pre-mining geomorphology and surface geology of the Beasley Creek Gold Mine, Laverton, WA. CSIRO Division of Exploration Geoscience, Restricted Report 26R, 39 pp.

Robertson, I.D.M. and Crabb, J. 1988. A case-hardened carbon steel swingmill. CSIRO Division of Exploration Geoscience Technical Files. 6 pp.

Robertson, I.D.M. and Gall, S.F. 1988. A mineralogical, geochemical and petrographic study of rocks of drillhole BCD1 from the Beasley Creek Gold Mine - Laverton, WA. CSIRO Division of Exploration Geoscience, Restricted Report MG 67R, 44 pp.

Vincent, E.A. 1978. Silver. In K.H. Wedepohl (ed). Handbook of Geochemistry. Springer-Verlag. New York.